AD-A046 276 ROCHESTER UNIV N Y DEPT OF MECHANICAL AND AEROSPACE--ETC F/G 3/2
SOLAR MAGNETO-ATMOSPHERIC WAVES AND PENUMBRAL WAVES.(U)
DEC 76 J H THOMAS, A H NYE, A CLARK F19628-75-C-0011

UNCLASSIFIED AFGL-TR-77-0017 NL

OF
AD
A046276

END
DATE
FILMED
12-77
DDC

AFGL-TR-77-0017

12

B.S.

SOLAR MAGNETO-ATMOSPHERIC WAVES AND PENUMBRAL WAVES

John H. Thomas
Alan H. Nye
Alfred Clark, Jr.

Department of Mechanical and Aerospace Sciences
University of Rochester
Rochester, New York 14627

22 December 1976

Final Report
(Period 1 September 1974 through 30 September 1976)

Approved for public release; distribution unlimited

AIR FORCE GEOPHYSICS LABORATORY
AIR FORCE SYSTEMS COMMAND
UNITED STATES AIR FORCE
HANSCOM AFB, MASSACHUSETTS 01731

UNCLASSIFIED

SECURITY CLASSIFICATION OF THIS PAGE (When Data Entered)

REPORT DOCUMENTATION PAGE

READ INSTRUCTIONS BEFORE COMPLETING FORM

1. REPORT NUMBER: AFGL-TR- 77-0017	2. GOVT ACCESSION NO.
3. RECIPIENT'S CATALOG NUMBER	
4. TITLE (and Subtitle): SOLAR MAGNETO-ATMOSPHERIC WAVES AND PENUMBRAL WAVES.	5. TYPE OF REPORT & PERIOD COVERED: Final Report. Period 1 Sept 1974-30 Sept 1976
	6. PERFORMING ORG. REPORT NUMBER
7. AUTHOR(s): John H. Thomas, Alan H. Nye, and Alfred Clark, Jr	8. CONTRACT OR GRANT NUMBER(s): F 19628-75-C-0011
9. PERFORMING ORGANIZATION NAME AND ADDRESS: Dept. of Mechanical and Aerospace Sciences, University of Rochester, Rochester, New York 14627	10. PROGRAM ELEMENT, PROJECT, TASK AREA & WORK UNIT NUMBERS: 62101F, 678100, 76490601
11. CONTROLLING OFFICE NAME AND ADDRESS: Air Force Geophysics Laboratory, Hanscom AFB, Massachusetts 01731, Monitor/Steven Musman/PH	12. REPORT DATE: December 22, 1976
	13. NUMBER OF PAGES: 49
14. MONITORING AGENCY NAME & ADDRESS (if different from Controlling Office): 51 p.	15. SECURITY CLASS. (of this report): Unclassified
	15a. DECLASSIFICATION/DOWNGRADING SCHEDULE

16. DISTRIBUTION STATEMENT (of this Report)

Approved for public release, distribution unlimited.

17. DISTRIBUTION STATEMENT (of the abstract entered in Block 20, if different from Report)

18. SUPPLEMENTARY NOTES

19. KEY WORDS (Continue on reverse side if necessary and identify by block number)

Magneto-atmospheric waves
Running penumbral waves
Sunspots
Coronal disturbances
Hydromagnetic stability

20. ABSTRACT (Continue on reverse side if necessary and identify by block number)

The linearized theory of magneto-atmospheric waves (involving the combined restoring forces due to buoyancy, compressibility, and magnetic field) is developed for the case of a horizontal magnetic field which may vary with height. The convective stability of the basic atmosphere is considered, and it is shown that a nonuniform horizontal magnetic field may be destabilizing as well as stabilizing.

(OVER)

→ Next page

DD FORM 1 JAN 73 1473 EDITION OF 1 NOV 65 IS OBSOLETE

UNCLASSIFIED

SECURITY CLASSIFICATION OF THIS PAGE (When Data Entered)

400 928

20. Abstract (continued)

A detailed model of a sunspot penumbra is studied in order to identify the mode of running penumbral waves. It is found that penumbral waves may be identified with magneto-atmospheric waves of the "plus" type that are vertically trapped at photospheric levels. Although most of the wave energy is contained in the penumbral photosphere and subphotosphere, the maximum vertical velocity occurs in the chromosphere where the waves are evanescent (and where they are observed in Hα).

An exact analytical solution for magneto-atmospheric wave modes is found in the case of an isothermal atmosphere permeated by a uniform horizontal magnetic field, without making the usual short-wavelength approximation. This solution is applied to an idealized model of the low-corona-chromosphere transition region as a model for flare-induced coronal waves. Disturbances propagate horizontally in the waveguide formed by the rapid density increase into the chromosphere below and the rapid increase in Alfvén speed into the corona above.

The exact solution mentioned above is also used in conjunction with a simple two-layer model of a sunspot penumbra to further study the mode of running penumbral waves. The lowest "plus" eigenmode of the model is in good agreement with observations of penumbral waves.

The theory of penumbral waves developed here predicts that these waves should be observable in the photosphere as well as the chromosphere. This prediction prompted a search for penumbral waves in the photosphere, carried out with the tower telescope and diode array at Sacramento Peak Observatory. Simultaneous observations have been made of velocities in the chromosphere (in Hα) and in the photosphere (in the nonmagnetic Fe I line λ5576) of three sunspots. The results reveal waves propagating horizontally outward across the penumbra in the photosphere with about the same period as the running penumbral waves in Hα (250-290 s). The photospheric waves are more intermittent and have higher horizontal phase velocity (by a factor of 2 or more) than the chromospheric penumbral waves. The connection between the photospheric and chromospheric penumbral waves is unclear at present, and in any case is more complicated than the resonant mode model presented here.

PERSONNEL

Air Force Contract F 19628-75-C-0011

John H. Thomas,	Principal Investigator
Alfred Clark, Jr.,	Faculty Associate
Alan H. Nye,	Research Assistant

CONTENTS

THE NATURE OF RUNNING PENUMBRAL WAVES

ALAN H. NYE* and JOHN H. THOMAS**
Max-Planck-Institut für Physik und Astrophysik, Munich, Germany

(Received 22 March; revised 25 June, 1974)

Abstract. A model of a sunspot penumbra, including the effects of magnetic field, compressibility, and buoyancy, is studied in order to identify the mode of running penumbral waves. It is found that the penumbral waves may be identified with gravity-modified magneto-acoustic waves of the 'plus' type that are vertically trapped at photospheric levels. Although most of the wave energy is contained in the penumbral photosphere and subphotosphere, the maximum vertical velocity occurs in the chromosphere where (i) the waves are evanescent and (ii) the vertical velocity is in fact observed (in Hα).

1. Introduction

Recent observations have disclosed an interesting pattern of velocity fields in sunspots. The most recent discovery is that of waves propagating radially outward in sunspot penumbrae (Zirin and Stein, 1972; Giovanelli, 1972). Zirin and Stein refer to these waves as running penumbral waves. With the further observations of Giovanelli (1974), we now have a fairly clear picture of the properties of these waves. The purpose of this theoretical paper is to study possible wave modes in a model of a sunspot penumbra in order to identify the mode of the running penumbral waves. We shall argue that the running penumbral waves are gravity-modified magneto-acoustic waves (of the 'plus' type) that are vertically trapped at photospheric levels.

Giovanelli (1974) has summarized the observations of running penumbral waves, and he presents the following picture. The waves are observed in Hα by means of their line-of-sight velocity. They occur in almost every sizable spot with a regular stable structure, but only rarely in active spots with complex structure. The waves travel outward in the penumbra at a typical speed of 15 km s^{-1}. The observed waves have periods in the range 180–240 s and horizontal wavelengths in the range 2350–3800 km. Observations near the limb have failed to reveal any horizontal motions associated with the penumbral waves, so the wave motion is predominantly vertical in Hα.

Thus far no detailed theoretical study of the mode of the running penumbral waves has appeared, although Moore (1973) has studied the related problem of the generation of penumbral waves in the umbra. Zirin and Stein (1972) tentatively identified the penumbral waves as sound waves, whereas Giovanelli (1972, 1974) identified them as Alfvén waves. The penumbral waves, with their predominant vertical motions, no doubt involve the combined effects of restoring forces due to compressibility, magnetic

* Also National Science Foundation Predoctoral Trainee, Dept. of Mechanical and Aerospace Sciences, University of Rochester, Rochester, N.Y., U.S.A.
** On leave of absence from the Dept. of Mechanical and Aerospace Sciences and the C. E. Kenneth Mees Observatory, University of Rochester, Rochester, N.Y., U.S.A.

Solar Physics **38** (1974) 399–413.

field, and buoyancy, and a complete theory should account for all three effects. This is done in the present paper.

In studying penumbral waves, we face a difficulty, in that there seems to be no complete, generally accepted penumbral model on which to base our calculations. We have therefore constructed a penumbral model for use in studying wave modes. This model (presented in Section 3), while simple enough to permit analysis of wave modes, nevertheless reproduces all of the relevant features of penumbral structure, and is in reasonable quantitative agreement with observations. We have assumed the penumbral magnetic field to be purely horizontal, but varying with height. True penumbral magnetic fields are not purely horizontal, although they may be very nearly so (Nishi and Makita, 1973). There is some disagreement over the inclination of the magnetic field in a penumbra (see Beckers and Schröter (1969) for a summary of observations). The assumption of a horizontal field here is mostly a matter of convenience; the basic mechanism we propose for the vertical trapping of penumbral waves will also work for an inclined field. We have also taken our model to be horizontally uniform – that is, we have not tried to represent the horizontal filamentary structure of a penumbra or the radial geometry.

In Section 2 we present the basic equations for waves in our model penumbral atmosphere. The basic atmosphere is completely characterized in these equations by the vertical distribution of three parameters: the sound speed c, the Alfvén velocity v_A, and the local density scale height H. In order to illustrate the properties of the various wave modes that can occur, we study the dispersion relation that holds in the case of constant c, v_A, and H. In Section 3 we present the basic penumbral model in terms of the distributions of c, v_A, and H with height. In Section 4 we show that the penumbral waves may be identified with 'plus' modes that are trapped in the photospheric-subphotospheric region in our model. We discuss these modes further in Section 5.

2. Basic Equations and Dispersion Relations

In our simplified treatment of a sunspot penumbra we shall ignore the radial spreading of magnetic field lines, and consider the undisturbed magnetic field to be purely horizontal (in the x-direction) and varying with height z; i.e., $\mathbf{B}_0 = (B_0(z), 0, 0)$. We assume the field permeates an inviscid, perfectly conducting, plane stratified atmosphere with constant acceleration of gravity g ($=0.274$ km s^{-2}) in the negative z-direction. The undisturbed pressure, density, and temperature are denoted by $p_0(z)$, $\varrho_0(z)$, and $T_0(z)$, respectively. The atmosphere is in hydrostatic equilibrium, so that

$$\frac{\mathrm{d}}{\mathrm{d}z}\left(p_0 + \frac{B_0^2}{8\pi}\right) = -\varrho_0 g\,. \tag{1}$$

We then consider small adiabatic perturbations of this equilibrium atmosphere. We consider wave vectors only in the xz plane, and assume that the perturbation velocity $\mathbf{u} = (u, v, w)$ has the form $\mathbf{u} = \hat{\mathbf{u}} \exp i(k_x x - \omega t)$, with $\hat{\mathbf{u}} = \hat{\mathbf{u}}(z) = (\hat{u}(z), \hat{v}(z),$

$\hat{w}(z)$). Starting with the linearized equations of continuity, energy, and momentum, we can eliminate the pressure and density perturbations, and arrive at the set of three linearized momentum equations for the velocity components $\hat{u}$, $\hat{v}$, and $\hat{w}$, in which the basic atmosphere is completely described by the sound speed $c(z)$, the Alfvén velocity $v_A(z)$, and the local density scale height $H(z)$, defined by

$$c^2 = \left(\frac{\partial p_0}{\partial \varrho_0}\right)_s, \qquad v_A^2 = \frac{B_0^2}{4\pi\varrho_0}, \qquad \frac{1}{H} = -\frac{1}{\varrho_0}\frac{\partial \varrho_0}{\partial z}. \tag{2}$$

The linearized momentum equations are the following:

$$(\omega^2 - c^2k_x^2)\,\hat{u} + ik_x c^2 \frac{d\hat{w}}{dz} - ik_x g\hat{w} = 0, \tag{3}$$

$$(\omega^2 - v_A^2 k_x^2)\,\hat{v} = 0, \tag{4}$$

$$(c^2 + v_A^2)\frac{d^2\hat{w}}{dz^2} + \left[\frac{d}{dz}(c^2 + v_A^2) - \frac{c^2 + v_A^2}{H}\right]\frac{d\hat{w}}{dz} + (\omega^2 - v_A^2k_x^2)\,\hat{w} + \\ + ik_x\left[\frac{dc^2}{dz} - \frac{c^2}{H} + g\right]\hat{u} + ik_x c^2\frac{d\hat{u}}{dz} = 0. \tag{5}$$

We can eliminate the horizontal velocity components $\hat{u}$ and $\hat{v}$ from the system of Equations (3)–(5) to obtain a single equation for the vertical velocity $\hat{w}$, in the form

$$\frac{d^2\hat{w}}{dz^2} + A(z)\frac{d\hat{w}}{dz} + B(z)\,\hat{w} = 0, \tag{6}$$

where

$$A(z) = -\frac{1}{H} + \left[\frac{\omega^4}{(\omega^2 - c^2k_x^2)}\frac{dc^2}{dz} + (\omega^2 - c^2k_x^2)\frac{dv_A^2}{dz}\right]\times \\ \times\left[v_A^2(\omega^2 - c^2k_x^2) + c^2\omega^2\right]^{-1} \tag{7}$$

and

$$B(z) = \left[(\omega^2 - v_A^2k_x^2)(\omega^2 - c^2k_x^2) - g\left(g - \frac{c^2}{H}\right)k_x^2 - \right. \\ \left. - g \times \frac{\omega^2k_x^2}{(\omega^2 - c^2k_x^2)}\frac{dc^2}{dz}\right]\left[v_A^2(\omega^2 - c^2k_x^2) + c^2\omega^2\right]^{-1}. \tag{8}$$

With the transformation

$$\phi(z) = \hat{w}(z)\exp\left[\tfrac{1}{2}\int_0^z A(z)\,dz\right] \tag{9}$$

Equation (6) assumes the form

$$\frac{d^2\phi}{dz^2} + f(k_x, \omega; z)\,\phi = 0, \tag{10}$$

where

$$f = B - \tfrac{1}{4}A^2 - \tfrac{1}{2}\frac{dA}{dz}. \tag{11}$$

Here, $|\phi|^2$ is roughly proportional to the kinetic energy of wave motion. Equation (10) is the propagation equation for waves in an atmosphere with vertically varying c^2, v_A^2, and H. For given distributions of $c^2(z)$, $v_A^2(z)$, and $H(z)$, we can use the expression for $f(z)$ (Equation (11)) to distinguish roughly between local regions where a wave with a particular frequency ω and horizontal wavelength k_x is vertically propagating ($f>0$) or vertically evanescent ($f<0$). We shall use this approach for our penumbral model in Section 4.

The simplest case to study is that of constant c^2, v_A^2, and H. We shall consider this case now in order to show the kinds of wave modes which can occur. Although this case does not apply strictly to a real penumbra, or in fact to our penumbral model, we can nevertheless apply the resulting dispersion relation locally to get an approximate picture of the wave modes. We can also approximate a continuous vertical variation of the parameters in the penumbra by a series of layers in which they are constant. In the case of constant c^2, v_A^2, and H, Equations (3)–(5) have constant coefficients, and we can assume a solution of the form $\hat{\mathbf{u}}(z)=\bar{\mathbf{u}}\exp(ik_z z+z/2H)$, where $\bar{\mathbf{u}}=(\bar{u},\bar{v},\bar{w})$ is a constant vector. Here, the factor $\exp(z/2H)$ accounts for the fact that, to conserve energy, the perturbation amplitude must grow as the density decreases. The system of Equations (3)–(5) then becomes (cf., Yu, 1965):

$$(\omega^2 - c^2k_x^2)\,\bar{u} + ik_x\left[ik_z c^2 - \left(g - \frac{c^2}{2H}\right)\right]\bar{w} = 0, \tag{12}$$

$$(\omega^2 - v_A^2 k_x^2)\,\bar{v} = 0, \tag{13}$$

$$ik_x\left[ik_z c^2 + \left(g - \frac{c^2}{2H}\right)\right]\bar{u} + \left[(\omega^2 - v_A^2k_x^2) - (c^2 + v_A^2)\times \left(k_z^2 + \frac{1}{4H^2}\right)\right]\bar{w} = 0. \tag{14}$$

The dispersion relation for waves is obtained from the condition for nonzero solutions of the homogeneous system (12)–(14), i.e., the vanishing of the determinant of the coefficients. This yields the dispersion relation

$$(\omega^2 - v_A^2k_x^2)\left\{\omega^4 - (c^2+v_A^2)\left(k_x^2 + k_z^2 + \frac{1}{4H^2}\right)\omega^2 + c^2v_A^2k_x^2\left(k_x^2 + k_z^2 + \frac{1}{4H^2}\right) - g\left(g - \frac{c^2}{H}\right)k_x^2\right\} = 0. \tag{15}$$

We now discuss the various wave modes given by this dispersion relation, with some comments on their relation to running penumbral waves.

2.1. THE PURE ACOUSTIC MODE

The dispersion relation (15) is satisfied with $\omega^2 = c^2 k_x^2$ for the particular imaginary value of k_z given by $ik_z = (1/2H) - (g/c^2)$. From Equations (12)–(14) we see the corresponding motion has $\bar{u} \neq 0$, whereas $\bar{v} = \bar{w} = 0$. This mode is thus a purely compressional, acoustic mode with dispersion relation identical to that of a homogeneous isothermal gas. This can occur since the motion is horizontal and parallel to the magnetic field, and thus there is no contribution from buoyant or magnetic forces. The amplitude behaves as

$$\dot{u} = \bar{u} \exp\left[\left(\frac{1}{H} - \frac{g}{c^2}\right) z\right],$$

and thus grows exponentially with height (since $H < c^2/g$ for stability of the unperturbed atmosphere (Yu, 1965)). The total momentum and energy are finite, however, provided there is a lower boundary confining the motion to a semi-infinite range of z. This mode is identical to the Lamb mode in the non-magnetic case, except that here the scale height H is modified by the magnetic field. Since this mode has no vertical motion, it can not be associated with the running penumbral waves.

2.2. THE PURE ALFVEN MODE

A root of the dispersion relation (15), for arbitrary k_z, is given by $\omega^2 = v_A^2 k_x^2$, which is the same as the dispersion relation for a pure Alfvén wave in a homogeneous atmosphere with uniform magnetic field. With $\omega^2 = v_A^2 k_x^2$, however, the other factor in the dispersion relation (15) is in general not zero, and thus Equations (12)–(14) show that the motion has $\bar{v} \neq 0$, whereas $\bar{u} = \bar{w} = 0$. The motion is purely horizontal and purely transverse to the magnetic field. Thus, the pure Alfvén mode in a stratified atmosphere is, so to speak, plane polarized, with no vertical motions. With $\bar{w} = 0$ there is no contribution from the buoyancy force, and, further, with $\bar{u} = 0$ the motion is incompressible, so the wave behaves as a pure Alfvén wave (with the amplitude factor $\exp(z/2H)$). Again, since this mode has no vertical motions, it can not be associated with the running penumbral waves. We turn now to the remaining roots of the dispersion relation (15), which do permit vertical motions.

2.3. THE PLUS AND MINUS MODES

The remaining roots of the dispersion relation (15) are given by

$$\omega_{\pm}^2 = \tfrac{1}{2}\left\{(c^2 + v_A^2)\left(k_x^2 + k_z^2 + \frac{1}{4H^2}\right) \pm \left[(c^2 + v_A^2)^2\left(k_x^2 + k_z^2 + \frac{1}{4H^2}\right)^2 - \right.\right.$$
$$\left.\left. - 4c^2 v_A^2 k_x^2\left(k_x^2 + k_z^2 + \frac{1}{4H^2}\right) + 4g\left(g - \frac{c^2}{H}\right)k_x^2\right]^{1/2}\right\}. \qquad (16)$$

We shall refer to these two modes as the 'plus' and 'minus' modes. These modes involve the interaction of all three restoring forces: buoyant, pressure, and magnetic.

They reduce to more familiar wave modes in certain limiting cases. For example, in the limit of vanishing magnetic field ($v_A \to 0$) they reduce to the acoustic and gravity modes of an isothermal atmosphere (see, for example, Thomas *et al.*, 1971). Alternatively, in the limit of no stratification ($H \to \infty$, $g \to 0$), they reduce to the fast and slow magnetoacoustic waves in a homogeneous atmosphere (see, for example, Osterbrock, 1961). For intermediate cases (such as for penumbral conditions), we can look at the modes as being either magnetically modified acoustic-gravity waves or gravity-modified magnetoacoustic waves. We shall continue to use the terms plus and minus modes here.

The plus and minus modes, for $k_z = 0$, are shown schematically in a diagnostic diagram in Figure 1. The asymptotic behavior of the dispersion relation (16) for $k_z = 0$ is such that

$$\omega_+^2 \to \frac{c^2 + v_A^2}{4H^2}, \qquad \omega_-^2 \to 0 \quad \text{for} \quad k_x \to 0, \tag{17}$$

and

$$\omega_+^2 \to k_x^2 \max(c^2, v_A^2), \quad \omega_-^2 \to k_x^2 \min(c^2, v_A^2) \quad \text{for} \quad k_x \to \infty. \tag{18}$$

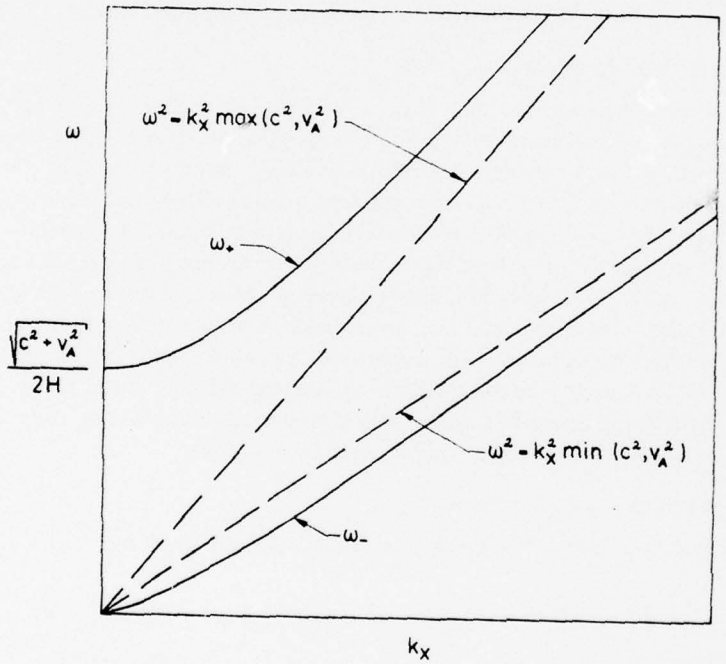

Fig. 1. Schematic diagnostic diagram of the plus and minus modes, showing curves for $k_z = 0$ (solid lines). The plus mode has a finite cutoff frequency as $k_x \to 0$. For $k_x \to \infty$, the plus and minus modes approach the dispersion lines for the pure acoustic and pure Alfvén modes. For strong stratification and weak magnetic field, the minus mode approaches the line $\omega = k_x v_A$ from above rather than below.

In the diagnostic diagram (Figure 1), there are vertically-propagating waves ($k_z^2 > 0$) above the ω_+ curve and below the ω_- curve, and evanescent waves ($k_z^2 < 0$) in the region between the two curves.

The plus mode has a finite cutoff frequency of $(\omega_+)_c = (c^2 + v_A^2)^{1/2}/2H$ as $k_x \to 0$. Estimates of this cutoff frequency at photospheric levels in a penumbra give values just a little lower than the frequencies of penumbral waves. This suggests that the penumbral waves might be identified with plus modes. We shall show this in more detail through the use of our penumbral model.

3. The Penumbral Model

We now present the penumbral model to be used in our wave calculations. For our purposes, a penumbral model consists of specified distributions of c^2, v_A^2, and H with height z. To simplify the calculations, we have chosen to represent the expected vertical variation of these parameters by piecewise linear functions. The specified forms of $c^2(z)$, $v_A^2(z)$, and $H(z)$ are shown in Figure 2. The important features of the model are as follows. The sound speed increases with depth into the convection zone from a broad minimum in the penumbral photosphere and chromosphere. The Alfvén velocity increases rapidly with height due to the nearly exponential decrease of density while the magnetic field decreases nearly linearly. The density scale height increases on either side of a minimum in the penumbral photosphere and low chromosphere. The model thus reproduces the main expected features of vertical penumbral structure. The numerical values of the parameters were chosen to represent a typical penumbra.

The distribution of the sound speed was determined primarily from the expected temperature distribution. Kjeldseth Moe and Maltby (1969) report that the temperature T in the penumbra may be obtained by adding a constant $\Delta\theta = 0.055$ to the θ values of the quiet photosphere, where $\theta = 5040/T$. With this $\Delta\theta$, the calculated relative intensities averaged over the penumbral fine structure agreed well with observations. Kjeldseth Moe and Maltby used the Bilderberg Continuum Atmosphere (Gingerich and de Jager, 1968) for their quiet photospheric temperatures; here, we use the more recent Harvard-Smithsonian Reference Atmosphere (HSRA, Gingerich *et al.*, 1971). Using the constant $\Delta\theta = 0.055$, the penumbral temperature minimum is found to be 3989 K, yielding a minimum value of the sound speed squared of $c^2 = 43.5\ \mathrm{km^2\ s^{-2}}$. The slope of the linear increase of c^2 into the convection zone was taken to be 0.1 $\mathrm{km\ s^{-2}}$; this choice is also based on the behavior of the HSRA. The distribution of sound speed (in $\mathrm{km\ s^{-1}}$) is given by

$$c^2(z) = \begin{cases} 63.5 - 0.1z & z \leqslant 200 \\ 43.5 & z > 200. \end{cases} \tag{19}$$

At some point in the penumbral chromosphere the sound speed will increase rapidly to coronal values. However, this increase takes place above the region where the penumbral waves are trapped in our model, so we have not included this in the model.

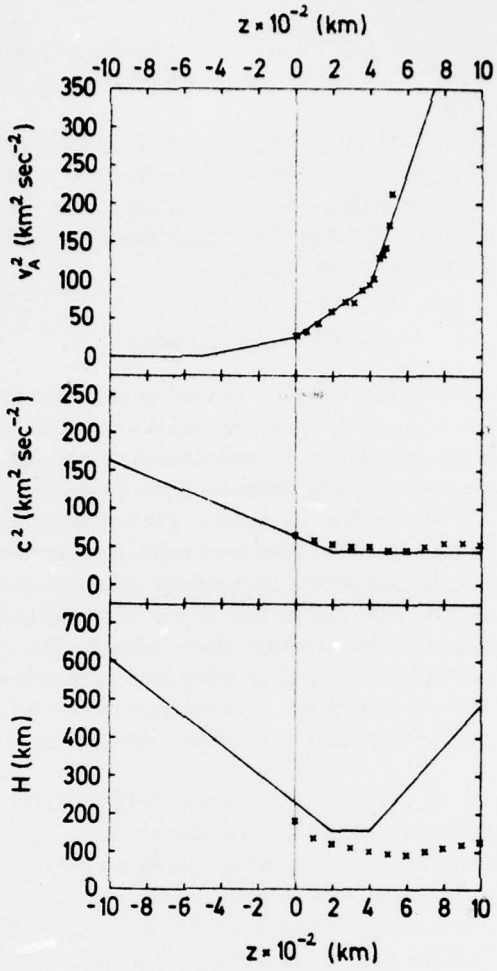

Fig. 2. Distribution of c^2, v_A^2, and H with height z in the penumbral model (solid lines). The data (crosses) for v_A^2 are based on penumbral observations (see text). Data points for quiet photospheric values of c^2 and H, based on the HSRA, are shown only for comparison with the penumbral model.

The distribution of c^2 is shown in Figure 2, along with quiet atmospheric values of c^2 from the HSRA (Nakagawa, 1973) for comparison.

To determine the Alfvén velocity, we assumed that the magnetic field strength decreases linearly with height and is 1000 G at $z=0$. The rate of decrease of field strength with height was taken to be 0.2 G km^{-1}, in accordance with observations (see Bray and Loughhead, 1964). The photospheric densities were estimated from the penumbral model of Makita (1963), the only penumbral model to give densities. His densities are consistent with more recent quiet photospheric models. The resulting

values of v_A^2 are plotted in Figure 2. The vertical distribution of these points was approximated in our model by two straight-line segments, with the upper segment extrapolated to greater heights. In the convection zone, the Alfvén velocity was approximated by another straight line segment which goes to zero at $z = -500$ km, due primarily to the increase in density with depth, but also to the fact that the penumbral field probably lies over the convection zone. The resulting distribution of the Alfvén velocity (in km s^{-1}) is given by

$$v_A^2(z) = \begin{cases} 0 & z < -500 \\ 25 + 0.05z & -500 \leqslant z < 0 \\ 25 + 0.172z & 0 \leqslant z \leqslant 400 \\ 94 + 0.75\,(z - 400) & z > 400\,. \end{cases} \tag{20}$$

The distribution of the local density scale height H (in km) with height was chosen to be

$$H(z) = \begin{cases} 230 - 0.375z & z < 200 \\ 155 & 200 \leqslant z < 400 \\ 155 + 0.55\,(z - 400) & z \geqslant 400\,. \end{cases} \tag{21}$$

In choosing values for H, we were guided by the following expression for the vertical entropy gradient in the atmosphere:

$$\frac{\mathrm{d}s}{\mathrm{d}z} = \frac{\varrho c_v \kappa}{\beta T}\left[\left(c^2 + \frac{v_A^2}{2}\right)\frac{1}{H} - g - \frac{\mathrm{d}}{\mathrm{d}z}\left(\frac{v_A^2}{2}\right)\right], \tag{22}$$

where c_v is the specific heat at constant volume, κ is the isothermal compressibility, and β is the coefficient of thermal expansion. This relation follows from the hydrostatic equation (1) and the basic thermodynamic relation

$$T\,\mathrm{d}s = \frac{\kappa c_v}{\beta}\,(\mathrm{d}p - c^2\,\mathrm{d}\varrho). \tag{23}$$

The distribution of H given in (21) is such that the entropy gradient $\mathrm{d}s/\mathrm{d}z$ is negative in the upper convection zone and positive in the penumbral photosphere and chromosphere. The distribution of H is shown in Figure 2, along with quiet atmospheric values of H from the HSRA (Nakagawa, 1973) for comparison. Here we can see the effect of the supporting magnetic field; the scale height is greater in the penumbra than in the quiet atmosphere. The effect of the magnetic field increases as the density decreases.

4. Trapping of Plus Modes in the Penumbral Photosphere

We now show that the running penumbral waves can be identified in our model with plus modes that are vertically trapped at photospheric levels. The basic mechanism for the trapping is the refraction due to (i) the increasing Alfvén velocity with increasing height in the photosphere-low chromosphere, and (ii) the increasing sound speed with depth in the convection zone. We shall demonstrate the trapping mechanism in two

ways: first, by considering the local dispersion relation (16) at three distinct levels in the model penumbra (assuming locally constant parameters), and second, by considering the propagation equation (10) for the complete continuous penumbral model (Figure 2).

4.1. THREE-LEVEL MODEL

A convenient method of looking at wave modes in our model is to draw diagnostic diagrams such as Figure 1 for various heights in the atmosphere, assuming locally constant values of c^2, v_A^2, and H – that is, ignoring the derivatives of these parameters in Equation (3)–(5). Although only approximate, this method does give some feeling for the behavior of the wave modes. We shall draw diagnostic diagrams for three different levels in our model penumbra; one in the convection zone, one in the photosphere, and one in the chromosphere. We may interpret these diagnostic

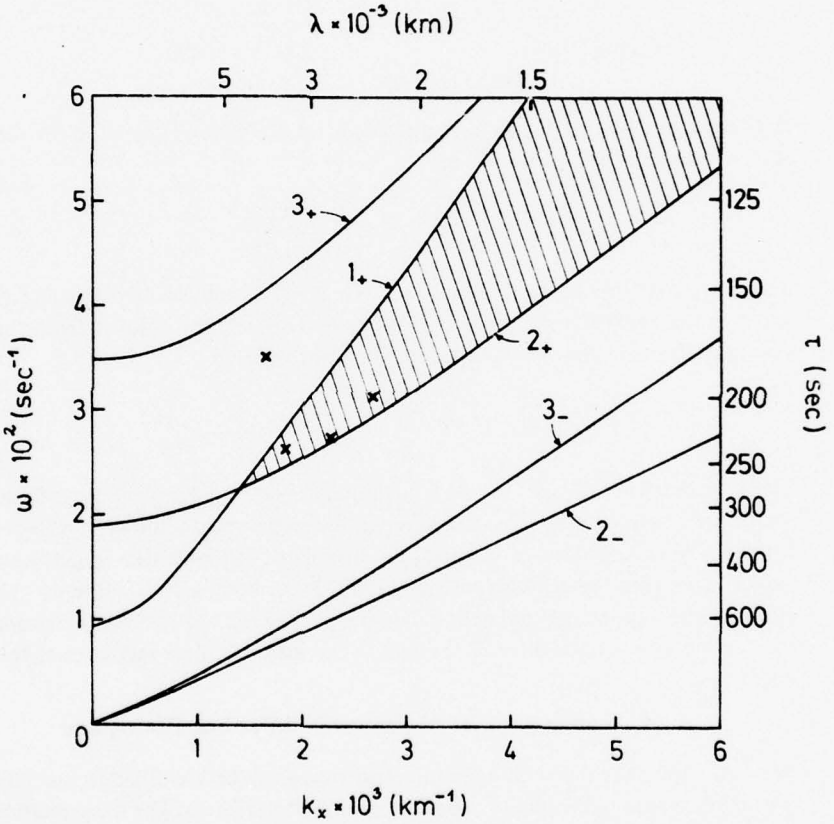

Fig. 3. Superimposed diagnostic diagrams for values of c^2, v_A^2, and H at three different levels in the model penumbra: level, 1 $z = -1400$ km; level 2, $z = -50$ km; level 3, $z = 500$ km. The shaded region is a region of vertical trapping of plus modes around level 2. The crosses correspond to observed running penumbral waves (Giovanelli, 1974).

diagrams more properly as representing a three-layer model of the penumbra, where in each layer the parameters are constant. A middle layer of finite thickness representing the penumbral photosphere is bounded above and below by semi-infinite layers representing the penumbral chromosphere and convection zone, respectively.

Figure 3 shows diagnostic diagrams for values of c^2, v_A^2, and H at three different levels in the penumbral model: $z = -1400$ km (layer 1, convection zone), $z = -50$ km (layer 2, penumbral photosphere), and $z = 500$ km (layer 3, penumbral chromosphere). The important feature of this figure is the existence of the shaded region in which the plus modes are vertically propagating in layer 2, but are vertically evanescent in layers 1 and 3. These modes are thus trapped in layer 2. The plus mode diagnostic curve for layer 3 lies above that of layer 2 because of the higher Alfvén velocity in layer 3. For higher levels in the chromosphere, the plus mode curve for layer 3 will be higher than that shown. The plus mode diagnostic curve for layer 1 has a lower cutoff frequency than layer 2 due to the larger scale height in the convection zone, but lies above the curve for layer 2 for higher values of k_x because of the higher value of c^2 in layer 1. For deeper levels in the convection zone, the plus mode curve for layer 1 will have an even lower cutoff frequency and a steeper slope. The existence of the region of trapping in the diagnostic diagram is a consequence of the qualitative features of our model and is not dependent on the particular choice of numerical values.

There is no trapping of minus modes in Figure 3. All the minus modes propagating in layer 2 are also propagating in layer 3. The minus mode curve for layer 1 has vanished since the Alfvén velocity is zero and the atmosphere is convectively unstable at that level.

Also shown in Figure 3 are four data points corresponding to penumbral waves observed in different sunspots by Giovanelli (1974) for which he gives specific wavelength and periods. These points tend to cluster in the long-wavelength end of the shaded region of trapping of the plus modes. The one point which lies outside the shaded region does lie in the region of trapping if the parameter values in layer 1 are chosen to represent a lower level in the convection zone. That is, a wave of this frequency and wavelength is reflected at a lower level in the convection zone in our model. This data point is considered atypical by Giovanelli, however. The observational data correspond to different sunspots, no doubt having different field strengths, whereas the diagnostic curves are for a single choice of the model parameters. Nevertheless, the resulting picture in Figure 3 clearly shows that the running penumbral waves should be identified with plus modes which are vertically trapped at photospheric levels in our model.

4.2. Continuous model

We now illustrate more accurately the trapping of the penumbral waves by making use of our complete penumbral model (Figure 2) in conjunction with the propagation equation (10). Roughly speaking, a wave is vertically propagating when the function $f(k_x, \omega; z)$ (Equation (11)) is positive, and is vertically evanescent when f is negative. In Figure 4 we have plotted f as a function of z for our penumbral model (Figure 2) for

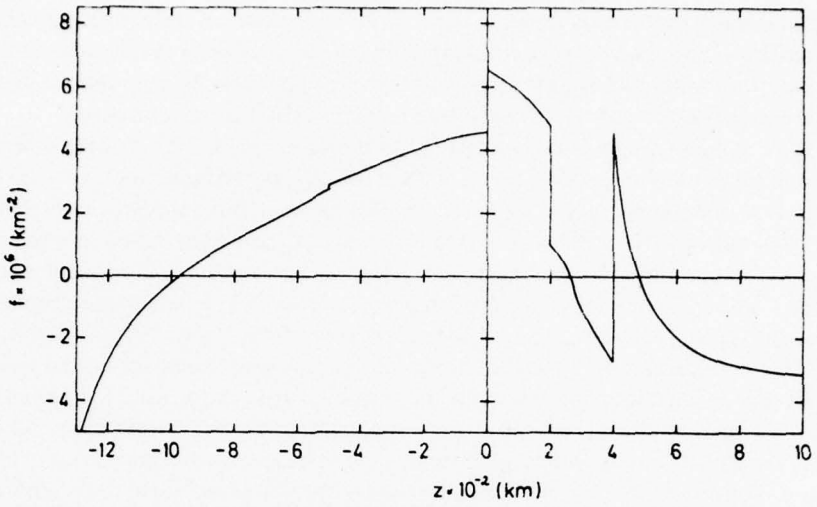

Fig. 4. The function $f(k_x, \omega; z)$ evaluated for the penumbral model (Figure 2) with $k_x = 2 \times 10^{-3}$ km^{-1}, $\omega = 3 \times 10^{-2}$ s^{-1}.

a typical value of horizontal wavenumber ($k_x = 2 \times 10^{-3}$ km^{-1}) and frequency ($\omega = 3 \times 10^{-2}$ s^{-1}) for penumbral waves. The function $f(z)$ is discontinuous due to the discontinuities in the first derivatives of the parameters c^2, v_A^2, and H in our model. The general behavior of f is that it is positive in a central region extending from $z \approx -1000$ km to roughly $z \approx 300$ km, and negative above and below this region.

In the lowest order WKB approximation, the general solution to (10) is given by

$$\phi(z) = \exp\left[\pm i \int_0^z \sqrt{f}\, dz\right]. \tag{24}$$

If f is positive for $0 < z < z_0$ and negative for $z > z_0$, then the solution for $z > z_0$ which is bounded as $z \to \infty$ can be written as

$$\phi(z) = \exp\left[\pm i \int_0^{z_0} \sqrt{f}\, dz - \int_{z_0}^z \sqrt{-f}\, dz\right]. \tag{25}$$

Thus, for $z > z_0$, the solution has the form of an exponential decay (with variable exponential factor), and the wave may be characterized as evanescent in the vertical direction. This analysis is somewhat crude, however, since the WKB solution (24) is not accurate in the neighborhood of z_0. The same analysis applies to the case where f is positive for $-z_0' < z < 0$ and negative for $z < -z_0'$. The wave then becomes evanescent as z decreases below $-z_0'$. Applying this to Figure 4, we conclude that a wave with the specified horizontal wavelength and frequency is trapped roughly in the

central region $-1000<z<300$ where f is positive. The exact location of the upper boundary of the trapping region is somewhat unclear due to the complicated discontinuous behavior of f there. This is due to the piecewise linear nature of our model; with smoother distributions of c^2, v_A^2, and H, the function f would have a single, smooth zero crossing at some $z>0$.

We have been discussing the behavior of the function $\phi(z)$. Comparison with the case of constant parameters shows that $|\phi|^2$ is roughly proportional to the kinetic energy of vertical motion of the wave ($\phi \sim \sqrt{\varrho}\, w$). Thus, it is the kinetic energy that is trapped in the region of positive f. The amplitude of the vertical velocity behaves somewhat differently. From Equations (9) and (25) we have, for $z>z_0$,

$$\hat{w}(z) = \exp\left[\pm i \int_0^{z_0} \sqrt{f}\, dz + Q(z)\right], \tag{26}$$

where

$$Q(z) = -\tfrac{1}{2}\int_0^z A\, dz - \int_{z_0}^z \sqrt{-f}\, dz. \tag{27}$$

The function $A(z)$ (Equation (7)) is negative over a range in z, and the function $Q(z)$ will remain positive over a range of z beyond z_0 before becoming negative. Thus, the vertical velocity continues to increase above z_0 before reaching a maximum at $z=z_1$, where z_1 is determined from the relation $Q(z_1)=0$. This can occur in spite of the decreasing energy above $z=z_0$ due to the rapid decrease in density.

By numerically evaluating the integrals in (27), we have estimated the point z_1 of maximum vertical velocity in our model, again for the choice $k_x = 2\times 10^{-3}$ km^{-1} and $\omega = 3\times 10^{-2}$ s^{-1}. The resulting value is $z_1 \approx 1250$ km. This is at a level where the wave is evanescent, and is well into the region of formation of Hα (Vernazza *et al.*, 1973). Thus, although the trapped waves have their maximum energy at lower levels ($z\approx 0$) where the density is higher, the vertical velocity is greatest at chromospheric levels where is it observed.

5. Discussion

An important conclusion that emerges from our model is that the running penumbral waves are basically a photospheric phenomenon, even though they are observed at chromospheric levels. This is really an expected result; the phase velocity of the penumbral waves is typical of photospheric conditions rather than chromospheric. For example, the Alfvén velocity at Hα levels in the penumbra is far greater than the phase velocity of the penumbral waves. In our picture, the waves are evanescent where they are observed. That is, the observed vertical motions are a passive response to an actively propagating wave at lower levels. We have shown that although the energy is trapped at photospheric levels, the vertical velocity reaches its maximum value at levels of formation of Hα, consistent with observations.

The concept of the penumbral waves as a photospheric phenomenon is also quite

consistent with their expected source of excitation. Moore (1973) has shown that the likely source of excitation of the penumbral waves is oscillatory convection in a subphotospheric layer in the umbra. The observation that the penumbral waves disappear suddenly at the boundary between the white-light penumbra and the surrounding photosphere also supports the photospheric nature of the waves. In the chromosphere, the penumbral fibril structure extends outward beyond this boundary.

The basic mechanism for the vertical trapping of the penumbral waves is not sensitive to the details of our penumbral model. This mechanism is based primarily on the increase in the sound speed as we go down into the convection zone and the increase in the Alfvén velocity as we go up into the chromosphere. These features are certain to remain in any improved penumbral model. Observationally, the insensitivity of the basic mechanism is confirmed by the fact that penumbral waves are seen in almost every stable, regular sunspot (Zirin and Stein, 1972).

The character of the trapped plus modes is different at different heights. The wave is more nearly acoustic at low levels (convection zone), but is more nearly Alfvénic at higher levels (photosphere and low chromosphere). The effect of stratification and gravity, while not dominant, is felt throughout the trapping region.

Although we have not attempted to calculate them, there are certainly resonant modes in our model which arise from the constructive interference of plus modes reflected from above and below in the trapping region. The resonant dispersion curves would lie in the shaded region in Figure 3. However, since the penumbral waves are a somewhat transitory phenomenon, there is no reason to associate them specifically with such a resonant mode; it is sufficient that a wave of the proper frequency and horizontal wavelength be vertically trapped.

Since our penumbral model is horizontally uniform, it cannot account for any observed horizontal (radial) variations in the penumbral waves. We can roughly account for the radial geometry of the penumbra by noting that the energy in a vertically trapped wave will decrease as $1/r$, where r is radius measured from the spot center, as the wave propagates radially outward. This accounts at least in part for the observed decrease in wave amplitude with radius. The sudden disappearance of the waves at the outer edge of the penumbra is associated with the more fundamental problem of the basic existence of the sharp boundary between the white-light penumbra and the surrounding photosphere.

Finally, we should note that our assumption of adiabatic perturbations is invalid over a limited range of height in the low photosphere, say the first few hundred kilometers above $z=0$. Here one should account for the rapid radiative exchange. The main effect of the radiative transfer on the plus modes is to effectively replace the adiabatic sound speed in this limited region by something nearer to the isothermal sound speed. The overall effect on the trapped plus modes discussed here will be quite small, even quantitatively.

Acknowledgements

This work was done during our one-year stay in the Max-Planck-Institut für Physik

und Astrophysik. We wish to thank Prof. Biermann for the hospitality of the Institut. We are grateful to Drs T. Hirayama, F. Meyer, and H. U. Schmidt for helpful discussions. This work was supported in part by the U.S. Office of Naval Research.

References

Beckers, J. M. and Schröter, E. H.: 1969, *Solar Phys.* **10**, 384.
Bray, R. J. and Loughhead, R. E.: 1964, *Sunspots*, Chapman and Hall, London, pp. 212–214.
Gingerich, O. and de Jager, C.: 1968, *Solar Phys.* **3**, 5.
Gingerich, O., Noyes, R. W., Kalkofen, W., and Cuny, Y.: 1971, *Solar Phys.* **18**, 347.
Giovanelli, R. G.: 1972, *Solar Phys.* **27**, 71.
Giovanelli, R. G.: 1974, in R. Grant Athay (ed.), 'Chromospheric Fine Structure', *IAU Symp.* **56**, 137.
Kjeldseth Moe, O. and Maltby, P.: 1969, *Solar Phys.* **8**, 275.
Makita, M.: 1963, *Publ. Astron. Soc. Japan* **15**, 145.
Moore, R. L.: 1973, *Solar Phys.* **23**, 403.
Nakagawa, Y.: 1973, *Solar Phys.* **33**, 87.
Nishi, K. and Makita, M.: 1973, *Publ. Astron. Soc. Japan* **25**, 51.
Osterbrock, D. E.: 1961, *Astrophys. J.* **134**, 347.
Thomas, J. H., Clark, P. A., and Clark, A., Jr.: 1971, *Solar Phys.* **16**, 51.
Vernazza, J. E., Avrett, E. H., and Loeser, R.: 1973, *Astrophys. J.* **184**, 605.
Yu, C. P.: 1965, *Phys. Fluids* **8**, 650.
Zirin, H. and Stein, A.: 1972, *Astrophys. J.* **173**, L85.

Convective instability in the presence of a nonuniform horizontal magnetic field

John H. Thomas* and Alan H. Nye*

Max-Planck-Institut für Physik und Astrophysik, München, Federal Republic of Germany
(Received 14 August 1974; final manuscript received 6 December 1974)

Newcomb's criterion for convective stability in the presence of a horizontal magnetic field is written in a form which explicitly shows the effect of vertical variations of the magnetic field strength. It is shown that a nonuniform horizontal magnetic field can be *destabilizing* as well as stabilizing.

We consider the convective instability of a compressible, inviscid, perfectly conducting gas permeated by a horizontal magnetic field $\mathbf{B}=[B(z),0,0]$ that may vary with height z, under a uniform gravitational acceleration g (in the negative z direction), assuming adiabatic perturbations. The first complete treatment of this problem was given by Newcomb[1] using the energy integral method. He showed that a necessary and sufficient condition for stability is given by

$$-\frac{d\rho}{dz} > \frac{\rho^2 g}{\gamma p}\ , \tag{1}$$

where ρ is mass density, p is pressure, and γ is the ratio of specific heats. In the case of instability, the most unstable mode has the form of an interchange of long but finite segments of magnetic field lines. The stability criterion (1) was also derived by Yu[2] by considering the force balance on a displaced magnetic flux tube.

Newcomb noted that the critical density gradient on the right-hand side of (1) is, at least explicitly, independent of the magnetic field, and is, in fact, that given by the Schwarzschild criterion[3] in the absence of a magnetic field. However, in the case of a nonuniform horizontal magnetic field (for which Newcomb's analysis is valid), the static distribution of pressure and density is affected by the magnetic field, and thus the stability criterion (1) depends implicitly on the magnetic field. This point, which was overlooked by Newcomb, will be pursued here.

Using the equation of hydrostatic equilibrium,

$$\frac{d}{dz}\left(p+\frac{B^2}{8\pi}\right) = -\rho g\ , \tag{2}$$

and the equation of state of a perfect gas, $p=\rho RT$, the stability criterion (1) can be written in the form

$$\frac{dT}{dz} - \left(\frac{dT}{dz}\right)_s > -\frac{1}{\rho R}\frac{d}{dz}\left(\frac{B^2}{8\pi}\right)\ , \tag{3}$$

where $(dT/dz)_s = -g/c_p = -g(\gamma-1)/\gamma R$ is the adiabatic temperature gradient. The new form (3) of the stability criterion has an advantage over the form (1) in that it shows *explicitly* the effect of vertical variations of the magnetic field, since the temperature distribution is independent of the magnetic field. For a uniform magnetic field ($B=$ const), (3) reduces to

$$\frac{dT}{dz} - \left(\frac{dT}{dz}\right)_s > 0,$$

which is identical to the Schwarzschild criterion in the absence of a magnetic field. [Note that usually, e.g., in a star, dT/dz and $(dT/dz)_s$ are both negative.] Thus, a uniform horizontal magnetic field has no effect on the condition for the onset of convective instability,[4] although, as Newcomb[1] also showed, it does have an effect on the growth rates of unstable modes.

If, however, the magnetic field is nonuniform, then (3) shows that the field can be stabilizing (in the case $dB/dz>0$) or destabilizing ($dB/dz<0$). A field that increases with height ($dB/dz>0$) can stabilize the atmo-

sphere in the presence of a superadiabatic temperature gradient. When the field decreases with height ($dB/dz < 0$), the critical temperature gradient is reduced below the adiabatic gradient.

As an illustration of the destabilizing effect for $dB/dz < 0$, consider the case of an isothermal atmosphere, which is convectively stable in the absence of a magnetic field. The stability criterion (3) reduces to

$$-\frac{1}{\rho}\frac{d}{dz}\left(\frac{B^2}{8\pi}\right) < -R\left(\frac{dT}{dz}\right)_s = g\left(\frac{\gamma-1}{\gamma}\right) . \tag{4}$$

If the magnetic pressure decreases more rapidly with height than the critical rate

$$\left[\frac{d}{dz}\left(\frac{B^2}{8\pi}\right)\right]_c = -\rho g\left(\frac{\gamma-1}{\gamma}\right) , \tag{5}$$

the atmosphere will be convectively unstable. For this critical magnetic field gradient, the corresponding pressure gradient is found from (2) to be

$$\left[\frac{dp}{dz}\right]_c = -\frac{\rho g}{\gamma} . \tag{6}$$

Thus, in the state of marginal stability in an isothermal atmosphere, the gradient of gas pressure balances the fraction $1/\gamma$ of the gravitational force, while the gradient of magnetic pressure balances the remaining fraction $(\gamma-1)/\gamma$ of the gravitational force.

A special case of interest is that of an isothermal atmosphere in which the field decreases with height in just the manner that causes the Alfvén speed $v_A = (B^2/4\pi\rho)^{1/2}$ to remain constant. In this case, (4) can be written as

$$\frac{v_A^2}{c^2} < 2\left(\frac{\gamma-1}{\gamma}\right) , \tag{7}$$

where $c = (\gamma RT)^{1/2}$ is the adiabatic sound speed. This stability criterion was obtained for this special case by Yu[5] from a normal mode analysis. Parker[6] has studied this case, including the effect of cosmic-ray pressure, in connection with the gaseous disk of the galaxy.

The destabilizing effect of a nonuniform magnetic field with $dB/dz < 0$ is similar to the phenomenon of "magnetic buoyancy" analyzed by Parker[7] and by Weiss.[8] Magnetic buoyancy is attributed to an isolated tube of magnetic flux in thermal equilibrium with its nonmagnetic surroundings. The instability discussed here is due to the buoyancy of an arbitrary tube of flux within a smoothly varying magnetic field.

This work was supported in part by the U.S. Office of Naval Research, and in part by the Air Force Cambridge Research Laboratories. One of us (AHN) was also supported in part by a National Science Foundation Predoctoral Fellowship.

*Permanent address: Department of Mechanical and Aerospace Sciences, University of Rochester, Rochester, N.Y. 14627.

[1]W. A. Newcomb, Phys. Fluids 4, 391 (1961).
[2]C. P. Yu, Phys. Fluids 9, 412 (1966).
[3]K. Schwarzschild, Nachr. K. Ges. Wiss. Gött., p. 41 (1906); see also M. Schwarzschild, *Structure and Evolution of the Stars* (Princeton University, Princeton, NJ, 1958), p. 44.
[4]This was also shown by R. J. Tayler, J. Nucl. Energy C 3, 266 (1961).
[5]C. P. Yu, Phys. Fluids 8, 650 (1965).
[6]E. N. Parker, Astrophys. J. 145, 811 (1966).
[7]E. N. Parker, Astrophys. J. 121, 491 (1955).
[8]N. O. Weiss, Mon. Not. R. Astron. Soc. 128, 225 (1964).

THE ASTROPHYSICAL JOURNAL, 204: 573–581, 1976 March 1

SOLAR MAGNETO-ATMOSPHERIC WAVES. I. AN EXACT SOLUTION FOR A HORIZONTAL MAGNETIC FIELD

ALAN H. NYE AND JOHN H. THOMAS*
Department of Mechanical and Aerospace Sciences, University of Rochester
Received 1975 June 20; revised 1975 August 7

ABSTRACT

The linearized theory of magneto-atmospheric waves (involving the combined restoring forces due to buoyancy, compressibility, and magnetic field) is developed for the case of a horizontal magnetic field. A general propagation equation is derived for adiabatic perturbations with arbitrary vertical distributions of the sound speed c, Alfvén velocity v_A, and local density scale height H. An exact analytical solution to the propagation equation is obtained for the case of an isothermal atmosphere permeated by a uniform horizontal magnetic field, without making the usual short-wavelength assumption. This solution is applied to an idealized model of the low-corona–chromosphere transition region for comparison with observations of flare-induced coronal waves. The results show that disturbances may propagate horizontally in the low corona in a wave guide formed by the sudden density increase into the chromosphere below and by the rapidly increasing Alfvén velocity with height in the corona. The group velocity of the guided wave modes is nearly independent of wavelength, so that a disturbance propagates as a compact wave packet.

Subject headings: hydromagnetics — Sun: atmospheric motions — Sun: corona — Sun: magnetic fields

I. INTRODUCTION

The theory of waves in a compressible, stratified, electrically conducting atmosphere permeated by a magnetic field is of considerable importance in astrophysics, especially in solar physics where there is a wealth of detailed observations of such waves in the solar atmosphere. Following Yu (1965), we shall refer to waves which involve compressibility, buoyancy, and magnetic forces as *magneto-atmospheric waves*. Among the many solar phenomena that are seemingly attributable to magneto-atmospheric waves are the heating of the corona and of chromospheric plages, the 5-minute oscillations in active regions, oscillations in sunspot umbrae and penumbrae, and flare-induced coronal disturbances.

The theory of magneto-atmospheric waves is complicated by the anisotropic nature of the medium; the gravitational field and the magnetic field each introduce preferred directions. Additionally, the disturbance is subjected to the combined restoring forces due to compressibility, buoyancy, and the magnetic field, so that pure wave modes (i.e., acoustic, Alfvén, and gravity) exist only as special cases. In general, magneto-atmospheric waves involve the effects of all three restoring forces. The problem is compounded by the fact that the basic parameters describing wave propagation in the solar atmosphere (the sound speed c, the Alfvén velocity v_A, and the local density scale height H) are, in general, functions of height, and therefore the disturbance cannot be represented by plane waves propagating in the atmosphere.

Previously, the problem of magneto-atmospheric waves has been studied by either of two basic approaches, each yielding a dispersion relation based on constant values of the atmospheric parameters. The first approach has been to assume that the vertical extent of the disturbance is much less than the smallest scale height for variation of the atmospheric parameters. The parameters can then be taken as constant locally. McLellan and Winterberg (1968) studied an isothermal atmosphere permeated by a uniform magnetic field with arbitrary orientation. Then, assuming that the Alfvén velocity is constant locally (although it actually increases exponentially with height), they derived a local dispersion relation that is valid for short wavelengths (short compared with the density scale height). This local dispersion relation has been studied by several authors (Bel and Mein 1971; Michalitsanos 1973; Nakagawa *et al.* 1973) to determine the effects of different propagation directions and magnetic field orientations.

The second basic approach has been to investigate an isothermal atmosphere permeated by a horizontal magnetic field that decreases exponentially with height such that the Alfvén velocity is constant, as are the sound speed and the density scale height. Yu (1965) derived the dispersion relation which in this case is valid for all wavelengths. He evaluated the three modes of propagation for various angles between the wave propagation vector and the magnetic field. Chen and Lykoudis (1972) used the dispersion relation of Yu to study the 5-minute oscillations in plage regions. Nye and Thomas (1974*a*) used Yu's dispersion relation in connection with a multilayer model for running penumbral waves.

* Also C. E. Kenneth Mees Observatory.

We consider only plane-parallel atmospheres, with no horizontal variation, in order to permit Fourier decomposition in the horizontal directions as well as time. With variations in the z-direction only, the governing partial differential equations reduce to ordinary differential equations. There are only two magnetic field configurations consistent with static equilibrium and no horizontal variation. They are $\boldsymbol{B}$ = constant and $\boldsymbol{B} = [B_x(z), B_y(z), 0]$. We shall restrict our study to the case of a unidirectional horizontal magnetic field that may vary with height. We shall not follow either of the two basic approaches discussed above, however, because of the inherent limitations of each of them for solar applications. The length scale for magnetic field changes in the solar atmosphere is generally much greater than the density scale height, so that the assumption of constant Alfvén velocity is not justified. On the other hand, the length scale of observed disturbances in the solar atmosphere is not generally small compared with the density scale height. This is especially true in the photosphere where the density scale height may be smaller than 100 km, and hence smaller than the limit of observational resolution.

In § II we derive a general propagation equation for an arbitrary direction of propagation and arbitrary vertical variations of the atmospheric parameters. For the case of an isothermal atmosphere permeated by a uniform horizontal magnetic field, the Alfvén velocity increases exponentially with height. In § III we obtain an exact general solution of the propagation equation in this case. We compute eigenmodes for the case of a rigid lower boundary in § IV, and apply this to a specific solar wave phenomenon, the flare-induced coronal waves, in § V.

The analytical treatment in §§ II and III also forms the basis of a following paper in which we deal with running penumbral waves.

II. BASIC EQUATIONS

The atmosphere is assumed to be a compressible, inviscid, perfectly conducting gas under a uniform acceleration of gravity $\boldsymbol{g}$ ($=0.274$ km s^{-2}) in the negative z-direction. The undisturbed magnetic field is taken in the x-direction and may vary with height z; i.e., $\boldsymbol{B}_0 = [B_0(z), 0, 0]$. The undisturbed pressure, density, and temperature may all be functions of height z, and are denoted by $p_0(z)$, $\rho_0(z)$, and $T_0(z)$, respectively. We shall see that wave propagation in the basic atmosphere may be completely characterized by the vertical variation of the sound speed $c(z)$, the Alfvén velocity $v_A(z)$, and the local density scale height $H(z)$, defined by

$$c^2 \equiv \left(\frac{\partial p_0}{\partial \rho_0}\right)_s , \qquad v_A{}^2 \equiv \frac{B_0{}^2}{4\pi\rho_0} , \qquad \frac{1}{H} \equiv -\frac{1}{\rho_0}\frac{d\rho_0}{dz} . \tag{1}$$

The unperturbed atmosphere is taken to be in static equilibrium:

$$\frac{d}{dz}\left(p_0 + \frac{B_0{}^2}{8\pi}\right) = -\rho_0 g . \tag{2}$$

If the magnetic field is a function of height z, then it has a role in the basic equilibrium of the atmosphere. We consider only stable atmospheres, which requires that

$$\frac{dT_0}{dz} - \left(\frac{dT_0}{dz}\right)_s > -\frac{1}{\rho_0 R}\frac{d}{dz}\left(\frac{B_0{}^2}{8\pi}\right) ,$$

where $(dT_0/dz)_s$ is the adiabatic temperature gradient and R is the gas constant (see Thomas and Nye 1975 for a recent discussion).

Consider small adiabatic perturbations of the equilibrium atmosphere, letting p, ρ, $\boldsymbol{u}$, and $\boldsymbol{B}$ denote the perturbations in pressure, density, velocity, and magnetic field, respectively. Then, the basic linearized equations of continuity, momentum, energy, and induction are

$$\frac{\partial \rho}{\partial t} + \nabla\cdot(\rho_0 \boldsymbol{u}) = 0 , \tag{3}$$

$$\rho_0 \frac{\partial \boldsymbol{u}}{\partial t} + \nabla p - \rho \boldsymbol{g} - \frac{1}{4\pi}[(\nabla \times \boldsymbol{B}_0) \times \boldsymbol{B} + (\nabla \times \boldsymbol{B}) \times \boldsymbol{B}_0] = 0 , \tag{4}$$

$$\frac{\partial p}{\partial t} + \boldsymbol{u}\cdot\nabla p_0 = c^2\left(\frac{\partial \rho}{\partial t} + \boldsymbol{u}\cdot\nabla\rho_0\right) , \tag{5}$$

$$\frac{\partial \boldsymbol{B}}{\partial t} - \nabla \times (\boldsymbol{u} \times \boldsymbol{B}_0) = 0 . \tag{6}$$

After taking the time derivative of the momentum equation (4), we may eliminate the perturbation quantities p, ρ, and $\boldsymbol{B}$ by using equations (3), (5), and (6). This leaves a single vector equation for the velocity perturbation $\boldsymbol{u} = (u, v, w)$:

$$\rho_0 \frac{\partial^2 \boldsymbol{u}}{\partial t^2} + \nabla\left[\rho_0 w\left(g + \frac{1}{8\pi\rho_0}\frac{dB_0^2}{dz}\right) - c^2\rho_0\nabla\cdot\boldsymbol{u}\right] + [(\boldsymbol{u}\cdot\nabla)\rho_0 + \rho_0\nabla\cdot\boldsymbol{u}]\boldsymbol{g}$$

$$- \frac{1}{4\pi}[[(\nabla\times\boldsymbol{B}_0)\times[\nabla\times(\boldsymbol{u}\times\boldsymbol{B}_0)] - \boldsymbol{B}_0\times\{\nabla\times[\nabla\times(\boldsymbol{u}\times\boldsymbol{B}_0)]\}]] = 0\,. \quad (7)$$

Next, we assume that the perturbation velocity has the form $\boldsymbol{u} = \hat{\boldsymbol{u}}\exp i(\boldsymbol{k}\cdot\boldsymbol{r} - \omega t)$, with $\hat{\boldsymbol{u}} = \hat{\boldsymbol{u}}(z) = [\hat{u}(z), \hat{v}(z), \hat{w}(z)]$ and $\boldsymbol{k}\cdot\boldsymbol{r} = k_x x + k_y y$. Then, using the definition of v_A^2, the three components of the momentum equation (7) become

$$(\omega^2 - c^2k_x^2)\hat{u} - c^2k_xk_y\hat{v} - ik_x\left(g - c^2\frac{d}{dz}\right)\hat{w} = 0\,, \quad (8)$$

$$-c^2k_xk_y\hat{u} + [\omega^2 - c^2k_y^2 - v_A^2(k_x^2 + k_y^2)]\hat{v} - ik_y\left[g - (c^2 + v_A^2)\frac{d}{dz}\right]\hat{w} = 0\,, \quad (9)$$

and

$$ik_x\left(\frac{dc^2}{dz} - \frac{c^2}{H} + g + c^2\frac{d}{dz}\right)\hat{u} + ik_y\left[\frac{d}{dz}(c^2 + v_A^2) - \frac{(c^2 + v_A^2)}{H} + g + (c^2 + v_A^2)\frac{d}{dz}\right]\hat{v}$$

$$+ (c^2 + v_A^2)\frac{d^2\hat{w}}{dz^2} + \left[\frac{d}{dz}(c^2 + v_A^2) - \frac{(c^2 + v_A^2)}{H}\right]\frac{d\hat{w}}{dz} + (\omega^2 - v_A^2k_x^2)\hat{w} = 0\,. \quad (10)$$

These are the linearized perturbation equations. They give important information about particle motions for various modes of propagation in the atmosphere.

The horizontal components of the perturbation velocity can be eliminated from the system of equations (8)–(10) to yield a single equation for the vertical velocity $\hat{w}$. The resulting equation is

$$\frac{d^2\hat{w}}{dz^2} + A(z)\frac{d\hat{w}}{dz} + B(z)\hat{w} = 0\,, \quad (11)$$

where the coefficient $A(z)$ and $B(z)$ are given by

$$A(z) = -\frac{1}{H} + \frac{\omega^4}{DE}(\omega^2 - v_A^2k_x^2)^2\frac{dc^2}{dz} + \frac{1}{D}\left[-\omega^4 + (\omega^2 - c^2k_x^2)(\omega^2 - v_A^2k_x^2)\left(1 + \frac{\omega^4}{E}\right)\right]\frac{dv_A^2}{dz} \quad (12)$$

and

$$B(z) = \frac{1}{D}\left\{\omega^6 - [(c^2 + v_A^2)(k_x^2 + k_y^2) + v_A^2k_x^2]\omega^4\right.$$

$$+ \left[v_A^2k_x^2(k_x^2 + k_y^2)(2c^2 + v_A^2) - g(k_x^2 + k_y^2)\left(g - \frac{c^2}{H}\right) + \frac{g}{H}v_A^2k_y^2\right]\omega^2$$

$$\left. - v_A^2k_x^2(k_x^2 + k_y^2)\left[c^2v_A^2k_x^2 - g\left(g - \frac{c^2}{H}\right)\right] - \frac{g}{E}(\omega^2 - v_A^2k_x^2)^2\omega^2(k_x^2 + k_y^2)\frac{dc^2}{dz} - \frac{\omega^6}{E}k_y^2g\frac{dv_A^2}{dz}\right\}. \quad (13)$$

Here, D and E are given by

$$D = (\omega^2 - v_A^2k_x^2)[\omega^2(c^2 + v_A^2) - c^2v_A^2k_x^2] \quad (14)$$

and

$$E = \omega^4 - (k_x^2 + k_y^2)[\omega^2(c^2 + v_A^2) - c^2v_A^2k_x^2]\,. \quad (15)$$

Equation (11) is a general equation for the vertical component of velocity for a perturbation propagating in an arbitrary direction, in an atmosphere with a horizontal magnetic field and arbitrary vertical distributions of c^2, v_A^2, and H. This propagation equation has been given previously (Nye and Thomas 1974*a*) in the case $k_y = 0$.

III. ISOTHERMAL ATMOSPHERE WITH A UNIFORM HORIZONTAL MAGNETIC FIELD

Now consider the case where the undisturbed temperature and magnetic field are constant with height. Since the magnetic field is uniform, it has no effect on the hydrostatic equilibrium of the atmosphere, and the equilibrium pressure and density both decrease exponentially with height. The sound speed and the density scale height are both constant, with values determined by the temperature of the atmosphere. The Alfvén velocity increases exponentially with height due to the decreasing density. The sound speed, density scale height, density, and Alfvén velocity are given by

$$c = (\gamma R T_0)^{1/2} = \text{const.}\,, \tag{16}$$

$$H = \frac{RT_0}{g} = \text{const.}\,, \tag{17}$$

$$\rho_0(z) = \rho_{00} e^{-z/H}\,, \tag{18}$$

and

$$v_A(z) = v_0 e^{z/2H}\,, \tag{19}$$

where ρ_{00} and v_0 are the values of the undisturbed density and Alfvén velocity at $z = 0$.

The nondimensional parameter $\beta^2 \equiv v_0^2/c^2$ is introduced as a measure of the relative importance of the restoring forces due to the magnetic field and to compressibility at the point $z = 0$. For values of $\beta^2 < 1$, there is a region of the atmosphere above $z = 0$ where compressibility has more importance as a restoring force than does the magnetic force, but in any case the magnetic field always becomes dominant as z becomes large.

In the remainder of this paper we shall consider only waves whose horizontal component of propagation is parallel to the magnetic field ($k_y = 0$). Using (16)–(19), we may write (11) as

$$[c^2\omega^2 + (\omega^2 - c^2k_x^2)v_0^2e^{z/H}]\frac{d^2\hat{w}}{dz^2} - \frac{c^2\omega^2}{H}\frac{d\hat{w}}{dz} + \left[(\omega^2 - c^2k_x^2)(\omega^2 - v_0^2e^{z/H}k_x^2) - g\left(g - \frac{c^2}{H}\right)k_x^2\right]\hat{w} = 0\,. \tag{20}$$

We define the nondimensional frequency Ω and the nondimensional horizontal wavenumber K by

$$\Omega \equiv H\omega/c\,, \qquad K \equiv Hk_x\,. \tag{21}$$

By transforming the dependent and independent variables according to

$$W = \hat{w}e^{zK/H}\,, \qquad x = \frac{\Omega^2}{\beta^2(K^2 - \Omega^2)}\,e^{-z/H}\,, \tag{22}$$

we may put equation (20) in the dimensionless form

$$x(1 - x)\frac{d^2W}{dx^2} + [C - (A + B + 1)x]\frac{dW}{dx} - ABW = 0\,, \tag{23}$$

with

$$A + B = C = 2K + 1\,, \qquad AB = \Omega^2 + K + \left(\frac{\gamma - 1}{\gamma^2}\right)\frac{K^2}{\Omega^2}\,. \tag{24}$$

Equation (23) is the standard form of the hypergeometric differential equation.[1] The solutions of this equation may be expressed in terms of hypergeometric functions, given for $|x| < 1$ by

$$F(A, B; C; x) = \frac{\Gamma(C)}{\Gamma(A)\Gamma(B)}\sum_{n=0}^{\infty}\frac{\Gamma(A + n)\Gamma(B + n)}{\Gamma(C + n)}\frac{x^n}{n!}\,. \tag{25}$$

The general solution of equation (23) may be written, for $|x| < 1$, in terms of the original variables z and $\hat{w}(z)$ as

$$\hat{w}(z) = D_1e^{-zK/H}F\left[A, B; C; \frac{\Omega^2}{\beta^2(K^2 - \Omega^2)}\,e^{-z/H}\right] + D_2e^{zK/H}\left[\frac{\beta^2(K^2 - \Omega^2)}{\Omega^2}\right]^{2K}F\left[A - C + 1, B - C + 1; 2 - C; \frac{\Omega^2}{\beta^2(K^2 - \Omega^2)}\,e^{-z/H}\right], \tag{26}$$

where D_1 and D_2 are arbitrary constants.

[1] The hypergeometric nature of the wave equation in this case was noted by us earlier (Nye and Thomas 1974*b*), and also independently by Adam (1975).

IV. EIGENMODES FOR A RIGID LOWER BOUNDARY

We now examine modes of propagation in the relatively simple case of an isothermal atmosphere with a uniform horizontal magnetic field, bounded from below by a rigid wall at $z = 0$. The general solution (26) is subject to boundary conditions at $z = 0$ [$x = \Omega^2/\beta^2(K^2 - \Omega^2)$] and at $z = \infty$ ($x = 0$).

As a condition at $z = \infty$, we require that the total energy of the perturbation be integrable over $0 \leq z < \infty$. The magnetic energy of the perturbation is proportional to the square of the velocity. Since

$$\lim_{x \to 0} F(\alpha, \beta; \gamma; x) = 1 , \tag{27}$$

we see from equation (26) that we must take $D_2 = 0$.

The second boundary condition is that the vertical velocity vanish at the rigid wall, i.e., $\hat{w} = 0$ at $z = 0$, i.e., at $x = \Omega^2/\beta^2(K^2 - \Omega^2)$. Provided

$$\left| \frac{\Omega^2}{\beta^2(K^2 - \Omega^2)} \right| < 1 , \tag{28}$$

we may apply this condition directly to equation (26) with $D_2 = 0$ to obtain the dispersion relation

$$F\left[A, B; C; \frac{\Omega^2}{\beta^2(K^2 - \Omega^2)} \right] = 0 . \tag{29}$$

If, however, (28) is not satisfied, then other representations of the general solution (26), valid for $|x| \geq 1$, must be used in order to apply the boundary condition at $z = 0$. For

$$\frac{\Omega^2}{\beta^2(K^2 - \Omega^2)} \geq 1 , \tag{30}$$

the interval $0 \leq x \leq \Omega^2/\beta^2(K^2 - \Omega^2)$ contains the regular singular point at $x = 1$, and no solution that satisfies the boundary conditions and is also regular at $x = 1$ is to be expected. For the range

$$\frac{\Omega^2}{\beta^2(K^2 - \Omega^2)} \leq -1 , \tag{31}$$

we may use analytic continuation to extend the general solution (26). The analytic continuation of (26) with $D_2 = 0$, valid for $x \leq -1$, is given by

$$\hat{w}(z) = D_1 e^{-zK/H} \left\{ \frac{\Gamma(C)\Gamma(B - A)}{[\Gamma(B)]^2} \left[\frac{\beta^2(\Omega^2 - K^2)}{\Omega^2} \right]^A e^{zA/H} F\left[A, 1 - B; 1 - B + A; \frac{\beta^2(K^2 - \Omega^2)}{\Omega^2} e^{z/H} \right] \right.$$
$$\left. + \frac{\Gamma(C)\Gamma(A - B)}{[\Gamma(A)]^2} \left[\frac{\beta^2(\Omega^2 - K^2)}{\Omega^2} \right]^B e^{zB/H} F\left[B, 1 - A; 1 - A + B; \frac{\beta^2(K^2 - \Omega^2)}{\Omega^2} e^{z/H} \right] \right\} . \tag{32}$$

Thus, for the range of parameters (31), the dispersion relation is given by

$$\frac{\Gamma(B - A)}{[\Gamma(B)]^2} \left[\frac{\beta^2(\Omega^2 - K^2)}{\Omega^2} \right]^A F\left[A, 1 - B; 1 - B + A; \frac{\beta^2(K^2 - \Omega^2)}{\Omega^2} \right]$$
$$+ \frac{\Gamma(A - B)}{[\Gamma(A)]^2} \left[\frac{\beta^2(\Omega^2 - K^2)}{\Omega^2} \right]^B F\left[B, 1 - A; 1 - A + B; \frac{\beta^2(K^2 - \Omega^2)}{\Omega^2} \right] = 0 . \tag{33}$$

The dispersion relation (eq. [29] or [33]) has been evaluated for various values of the nondimensional parameter β^2. Examples are plotted in Figures 1 and 2 (also see Fig. 4). The curves in these figures represent well-defined eigenmodes of wave propagation in the atmosphere. These curves represent trapped waves propagating horizontally in the wave guide formed by the solid boundary below and the exponentially increasing Alfvén velocity above.

There are several ways of interpreting the effect of changing β^2 on the dispersion relation. First, different values of β^2 can be taken to represent the same magnetic field strength and the same density at $z = 0$, but different atmospheric temperatures. A second interpretation is that different values of β^2 represent the same magnetic field strength and the same temperature, but different densities. This is equivalent to placing the solid lower boundary at successively higher levels in the atmosphere corresponding to larger values of β^2. At each higher level the magnetic restoring force becomes more important due to the decreased density, while the compressible restoring force remains the same.

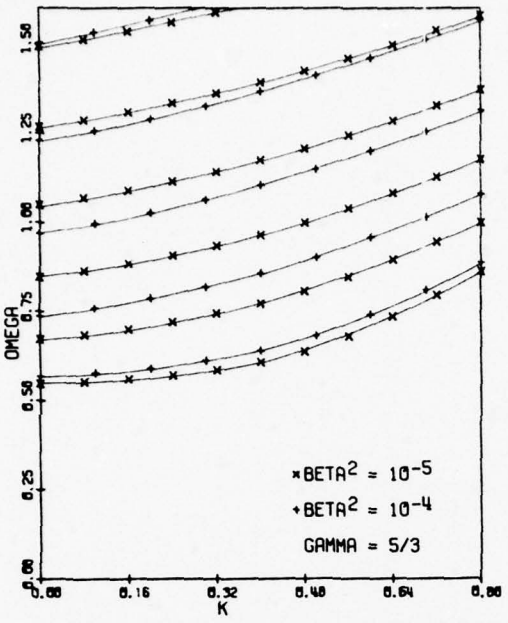

FIG. 1

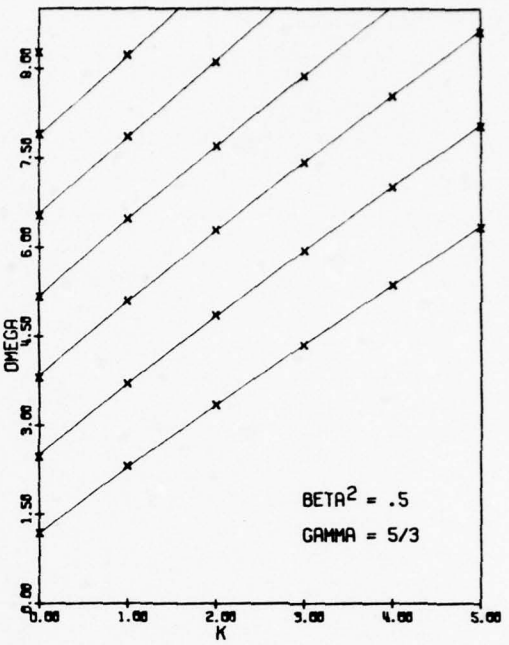

FIG. 2

FIG. 1.—Dispersion diagrams (nondimensional frequency versus nondimensional horizontal wavenumber) for an isothermal atmosphere with a uniform horizontal magnetic field and a solid lower boundary, with $\gamma = 5/3$, $\beta^2 = 10^{-5}$, and $\beta^2 = 10^{-4}$. The curves represent eigenmodes, and the crosses indicate the computed points. This figure should not be confused with a diagnostic diagram for an atmosphere with constant parameters (e.g., Yu 1965).

FIG. 2.—Same as Fig. 1, but with $\beta^2 = 0.5$.

The third interpretation is to consider changes in β^2 to be due to changes in the magnetic field strength, with fixed values of temperature and density. Since the sound speed and the density scale height then do not change, the scales for the frequency and horizontal wavenumber are the same in each case and the dispersion diagrams can be compared directly. From Figures 1 and 2 it can be seen that increasing the magnetic field strength (increasing β^2) increases the cutoff frequency. As β^2 increases, the slope of the dispersion curves, and hence the group velocity, also increases.

Lowering the value of γ to represent crudely the effect of radiative transfer has little effect on the nondimensional dispersion diagrams. However, the frequency scaling depends on γ as $\omega \sim (\gamma)^{1/2}\Omega$, while the wavenumber scaling is independent of γ. Therefore, for lower γ (lower sound speed) the wave oscillates less rapidly and the phase and group velocities are correspondingly lower.

The vertical velocity of the disturbance (eq. [26] or [32]) can be calculated as a function of height for any point on a dispersion curve. Figure 3 compares the lowest mode of oscillation for the same horizontal wavenumber but different values of β^2 (i.e., different magnetic field strengths), and shows that for increasing magnetic field strength, the wave oscillates more rapidly and is trapped at lower levels in the atmosphere. We now discuss the eigenmodes given by the dispersion relation (29) or (33) in relation to an observed solar oscillation.

V. APPLICATION TO FLARE-INDUCED CORONAL WAVES

On 1963 September 20, Moreton and Ramsey (Moreton 1965) observed a chromospheric disturbance, apparently caused by the flash phase of a flare, propagate at a nearly constant velocity of 750 km s^{-1} for several hundred thousand kilometers across the solar disk. Many other flare-induced disturbances have been reported (Moreton 1960; Athay and Moreton 1961; Dodson and Hedeman 1968), and the propagation velocity is usually on the order of 1000 km s^{-1}. Dodson and Hedeman (1968) report that the width of the disturbance created by the proton flare of 1966 August 28 was greater than 100,000 km.

These disturbances could not have been propagating solely in the chromosphere, since in the chromosphere the sound speed is only of the order of 20 km s^{-1} and the Alfvén velocity is only of the order of 50 km s^{-1}. Thus a purely chromospheric disturbance would have created a shock wave and been rapidly dissipated. In the corona, however, both the Alfvén velocity and the sound speed are an order of magnitude higher than in the chromosphere due to the increased temperature and decreased density. It has been proposed (Meyer 1968; Uchida 1968, 1970,

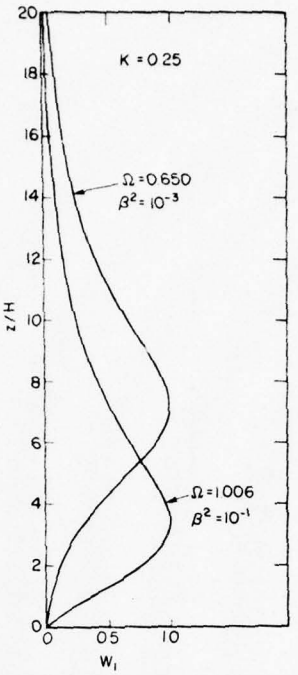

FIG. 3.—Direct comparison of the first mode of oscillation of the atmosphere for the same nondimensional horizontal wavenumber ($K = 0.25$) but for two values of β^2 ($\beta^2 = 10^{-3}$, $\beta^2 = 10^{-1}$).

1974; Uchida *et al.* 1973) that the disturbance is a magnetohydrodynamic wave propagating in the low corona and that the motion of this wave at the corona-chromosphere transition region is what is actually observed. There is, however, no general agreement as to the wavelength of the disturbance or even whether the observed disturbance is a single wave or a wave packet.

Meyer (1968) studied the propagation of the magnetoacoustic fast mode in an isothermal corona permeated by a uniform vertical magnetic field, with a rigid lower boundary representing the chromosphere-corona transition region. He found eigenmodes with nearly constant horizontal group velocity. Equating the group velocity to the observed propagation velocity, Meyer found that for a horizontal wavelength on the order of 100,000 km, the coronal magnetic field must be approximately 6 gauss, a reasonable average value.

Uchida, in a series of papers (Uchida 1968, 1970, 1974; Uchida *et al.* 1973), studied the propagation of short-wavelength (~ 5000 km) disturbances in various realistic coronal models. Using a ray-tracing technique, he obtained horizontal and vertical refractions in close agreement with the observed waves.

Although the magnetic field structure of the corona is quite complicated, the field changes fairly slowly and there are probably regions of nearly uniform field with almost any orientation. We study the case of a uniform horizontal field in connection with the coronal wave problem only as a means of understanding the mechanism of wave propagation for waves of arbitrary wavelength. Our model supplements Meyer's (1968) work by considering the case of a uniform horizontal magnetic field, and by including effects of gravity and stratification. As in Meyer's model, we use the rigid lower boundary to represent upward reflection from the chromosphere-corona transition layer.

We have evaluated our solution for a temperature of 1.6×10^6 K and $\beta^2 = 10$, which is fairly typical of the base of the corona. These values correspond to a sound speed of 180 km s^{-1} and a density scale height of approximately 71,000 km. Figure 4 shows the dimensional dispersion relation for these parameters. We see that the dispersion curves are nearly straight, which means that these modes have very little dispersion and will propagate for great distances with little change in character. The first three modes have been calculated for a wavelength of 75,000 km in Figure 5. The first mode has nearly zero vertical velocity above two scale heights and is therefore trapped in the low corona.

The phase velocity and group velocity of the first mode have been plotted as a function of horizontal wavenumber in Figure 6. For any wavelength of 100,000 km or less, the group velocity is nearly constant at about 610 km s^{-1}. Since the energy of a disturbance propagates at the group velocity, it is not important which specific wavelength, or spectrum of wavelengths, receives energy from the flare. The energy at all wavelengths will propagate together as a wave packet near the lower coronal boundary.

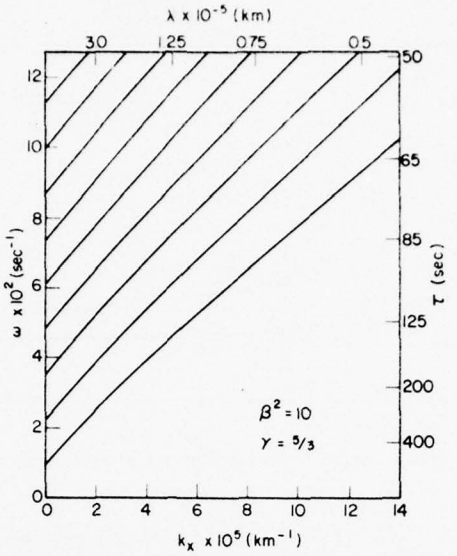

FIG. 4.—Dimensional dispersion diagram for $\beta^2 = 10$, $\gamma = 5/3$, and $T_0 = 1.6 \times 10^6$ K. The curves represent eigenmodes of the corona which are trapped by the increasing Alfvén velocity with height.

The present model is not proposed as a realistic model of the solar corona, although it may be fairly accurate over certain regions. No attempt has been made to include the effects of horizontal variations. The value of the model is that a mechanism for wave propagation can be studied for arbitrary wavelengths. These results close the gap between the short-wavelength ray-tracing theory and the long wavelength, vertical field case. We show that the question of wavelength is not particularly important since the group velocity of the trapped modes is essentially independent of wavelength. For the relatively large value of β^2 ($= 10$), the wave modes are basically the magneto-acoustic fast modes (studied by Meyer and by Uchida) modified by gravity. For an inclined magnetic field, there must also be trapped modes of propagation involving a coupling of the present modes and the type of mode studied by Meyer for a vertical field. The present results, taken with those of Meyer and the work of Uchida, present a consistent picture of flare-induced coronal waves as guided magneto-atmospheric waves.

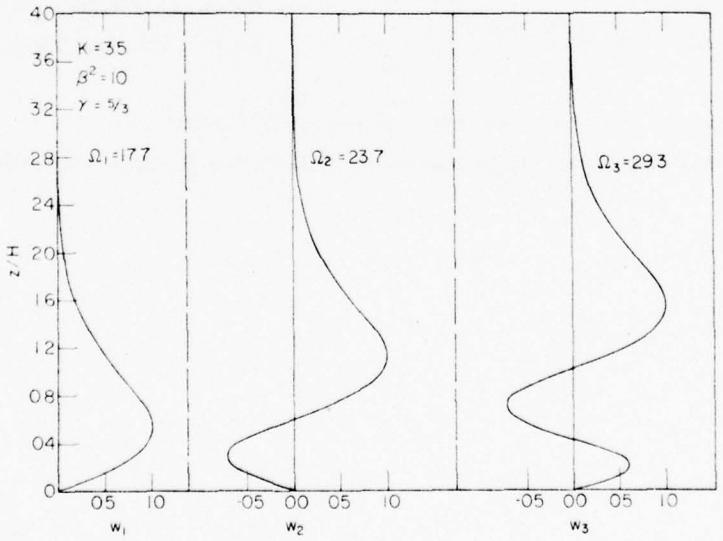

FIG. 5.—First three modes of oscillation of the model corona for $\beta^2 = 10$, $\gamma = 5/3$. The vertical velocities have been normalized to maximum value unity.

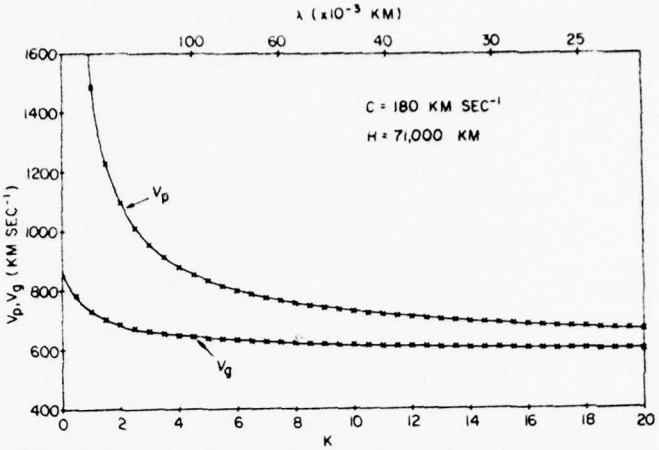

FIG. 6.—Phase velocity v_p and group velocity v_g of the first mode of coronal oscillation plotted as a function of horizontal wavenumber.

Much of this work was done while we were guests of the Max-Planck-Institut für Physik und Astrophysik in München, Germany. We are grateful to Professor Biermann for the hospitality of the Institut, and to Drs. H. U. Schmidt, Friedrich Meyer, John Stewart, and Tadashi Hirayama for helpful discussions. We also thank Professor Alfred Clark, Jr., at Rochester for helpful comments. One of us (A. H. N.) was supported by a National Science Foundation Predoctoral Traineeship. This work was supported by Air Force contract F 19628-75-C-0011 through Sacramento Peak Observatory, and by the Office of Naval Research.

REFERENCES

Adam, J. A. 1975, Ph.D. thesis, University of London.
Athay, R. G., and Moreton, G. E. 1961, *Ap. J.*, **133**, 935.
Bel, N., and Mein, P. 1971, *Astr. and Ap.*, **11**, 234.
Chen, J. C., and Lykoudis, P. S. 1972, *Solar Phys.*, **25**, 380.
Dodson, H. W., and Hedeman, E. R. 1968, *Solar Phys.*, **4**, 229.
McLellan, A., and Winterberg, F. 1968, *Solar Phys.*, **4**, 401.
Meyer, F. 1968, in *IAU Symposium 35, Structure and Development of Solar Active Regions*, ed. K. Kiepenheuer (Dordrecht: Reidel), p. 485.
Michalitsanos, A. G. 1973, *Solar Phys.*, **30**, 47.
Moreton, G. E. 1960, *A.J.*, **65**, 494.
Moreton, G. E. 1965, in *IAU Symposium 22, Stellar and Solar Magnetic Fields*, ed. R. Lüst (Amsterdam: North-Holland), p. 371.
Nakagawa, Y., Priest, E. R., and Wellck, R. E. 1973, *Ap. J.*, **184**, 931.
Nye, A. H., and Thomas, J. H. 1974*a*, *Solar Phys.*, **38**, 399.
———. 1974*b*, *Bull. Am. Phys. Soc.*, **19**, 1148.
Thomas, J. H., and Nye, A. H. 1975, *Phys. Fluids*, **18**, 490.
Uchida, Y. 1968, *Solar Phys.*, **4**, 30.
———. 1970, *Pub. Astr. Soc. Japan*, **22**, 341.
———. 1974, *Solar Phys.*, **39**, 431.
Uchida, Y., Altsuchuler, M. D., and Newkirk, G., Jr. 1973, *Solar Phys.*, **28**, 495.
Yu, C. P. 1965, *Phys. Fluids*, **8**, 650.

ALAN H. NYE: Sacramento Peak Observatory, Sunspot, NM 88349

JOHN H. THOMAS: Department of Mechanical and Aerospace Sciences, University of Rochester, Rochester, NY 14627

THE ASTROPHYSICAL JOURNAL, 204:582–588, 1976 March 1

SOLAR MAGNETO-ATMOSPHERIC WAVES. II. A MODEL FOR RUNNING PENUMBRAL WAVES

ALAN H. NYE AND JOHN H. THOMAS*
Department of Mechanical and Aerospace Sciences, University of Rochester
Received 1975 June 20

ABSTRACT

A simple two-layer model of a sunspot penumbra is used to study the mode of running penumbral waves. Exact solutions of the linearized wave equation, not limited to the small-wavelength approximation, are employed in each layer. The lowest "plus" eigenmode of magneto-atmospheric waves in the model penumbra is in good agreement with observations of running penumbral waves. The results indicate that running penumbral waves should be observable in a photospheric spectral line.

Subject headings: hydromagnetics — Sun: atmospheric motions — Sun: magnetic fields — Sun: sunspots

I. INTRODUCTION

In Paper I of this series (Nye and Thomas 1976) we presented an exact analytical solution for magneto-atmospheric waves in the case of an isothermal atmosphere with a uniform horizontal magnetic field. In the present paper we apply this solution to a simple two-layer model penumbra in order to study the mode of running penumbral waves.

Running penumbral waves (Zirin and Stein 1972; Giovanelli 1972, 1974; Moore and Tang 1975) are good examples of magneto-atmospheric waves. These waves propagate radially outward across sunspot penumbrae, with predominantly vertical motions in Hα. The observed range of frequency and propagation speed is fairly well established (see discussion in § IV).

Moore (1973) has concluded that the source of excitation of the penumbral waves is overstable convection in the low umbra. In an earlier paper (Nye and Thomas 1974 [NT]) we studied the mode of propagation of penumbral waves on the basis of a piecewise linear model of the vertical structure of a typical sunspot penumbra. We found the penumbral waves to be magneto-atmospheric waves (of the "plus" type) that are vertically trapped at photospheric levels. This trapping is primarily due to the increasing sound speed with depth into the convection zone and the increasing Alfvén velocity with height into the chromosphere.

Here we extend our earlier work by computing actual eigenmodes of propagation for a somewhat simpler model penumbra, which nevertheless retains the essential features. The properties of the lowest mode of propagation of the model penumbra turn out to be in good agreement with observations, and give some useful clues for further observation of running penumbral waves.

II. THE TWO-LAYER PENUMBRAL MODEL

The entire penumbral model consists of a compressible, inviscid, perfectly conducting, stratified perfect gas subject to a constant acceleration of gravity g ($=0.274$ km s^{-2}) in the negative z-direction. The upper layer is isothermal and is permeated by a uniform horizontal magnetic field, which yields an Alfvén velocity that increases exponentially with height due to the decreasing density. An exact solution of the linearized propagation equation for this case was given in Paper I.

This upper layer is a suitable model of the penumbral photosphere and chromosphere, where observed penumbral magnetic fields are very nearly horizontal (Nishi and Makita 1973) and decrease slowly with height (Bray and Loughhead 1964). The scale height for variation of the magnetic field is very large compared to the density scale height, so the assumption of the uniform horizontal magnetic field is reasonable. Our earlier calculations (NT) showed that running penumbral waves are trapped at photospheric levels, so that the increasing sound speed in the upper chromosphere has little effect on the trapping. Taking the upper layer to be isothermal is therefore also a reasonable assumption.

The vertical distributions of the sound speed and Alfvén velocity for the two-layer model penumbra are shown in Figure 1. Subscripts 1 and 2 denote quantities in the upper and lower layers, respectively, and the subscript 0

* Also C. E. Kenneth Mees Observatory.

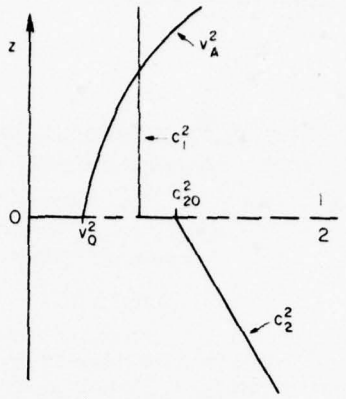

FIG. 1.—Distribution of c^2 and v_A^2 with height z in the two-layer penumbral model. The upper layer (1) is isothermal with a uniform horizontal magnetic field. The lower layer (2) has an adiabatic temperature gradient and no magnetic field.

refers to quantities evaluated at $z = 0$. The sound speed, density scale height, and Alfvén velocity in the upper layer are given by

$$c_1^2 = \gamma_1 R T_1 = \text{const.}, \tag{1}$$

$$H_1 = \frac{c_1^2}{\gamma_1 g} = \text{const.}, \tag{2}$$

and

$$v_A^2(z) = v_0^2 \exp(z/H_1). \tag{3}$$

The lower layer of the penumbral model (layer 2, figure 1) is adiabatic with no magnetic field. The temperature decreases with height (increases with depth) at the adiabatic lapse rate, $(dT/dz)_s = -g/c_p$, and thus this layer is neutrally stable. The actual temperature distribution in the convection zone below a penumbra is probably very nearly adiabatic, except for a thin superadiabatic layer just beneath the photosphere that we neglect here. There is no magnetic field in this layer since we assume that the penumbral magnetic field lies over the convection zone. The sound speed squared and local density scale height each increases linearly with depth in the lower layer, their functional forms being

$$c_2^2(z) = c_{20}^2 - g(\gamma_2 - 1)z \tag{4}$$

and

$$H_2(z) = H_{20} - (\gamma_2 - 1)z. \tag{5}$$

The corresponding density distribution is

$$\rho_2(z) = \rho_{20}[1 - (\gamma_2 - 1)z/H_{20}]^{1/(\gamma_2 - 1)}. \tag{6}$$

At the interface between the two layers ($z = 0$), we require the undisturbed density to be continuous to avoid introducing interfacial gravity waves and wave reflections; therefore, $\rho_{10} = \rho_{20}$. In the unperturbed penumbra, there must be pressure equilibrium at the interface; that is, the gas pressure in the lower layer at $z = 0$ must equal the sum of the gas pressure and the magnetic pressure in the upper layer at $z = 0$. Therefore, the gas pressure is greater in layer 2 than in layer 1; and since the density is continuous across the interface, the temperature is greater in layer 2. This may be expressed in terms of the sound speeds and the Alfvén velocity at $z = 0$ as

$$c_{20}^2 = \frac{\gamma_2}{\gamma_1} c_1^2 + \frac{\gamma_2}{2} v_0^2. \tag{7}$$

We now turn to the problem of computing eigenmodes of magneto-atmospheric waves in this penumbral model.

III. ANALYSIS

Consider first the behavior of small adiabatic perturbations in the lower layer (layer 2), an adiabatic atmosphere without magnetic field. Leibacher (1971) solved this problem in his study of oscillations of the quiet photosphere. Here we take a slightly different approach from his, using other transformations which yield a different form of the

propagation equation. For vanishing magnetic field ($\boldsymbol{B}_0 = \boldsymbol{B} = 0$), the vector equation for the perturbation velocity (eq. [7], Paper I) becomes

$$\frac{\partial^2 \boldsymbol{u}_2}{\partial t^2} = c_2^2 \nabla\phi + (\gamma_2 - 1)\phi \boldsymbol{g} + \nabla(\boldsymbol{u}_2 \cdot \boldsymbol{g}), \tag{8}$$

where $\phi = \nabla \cdot \boldsymbol{u}_2$.

We assume that the perturbation velocity has the form $\boldsymbol{u}_2 = \hat{\boldsymbol{u}}_2(z) \exp[i(k_x x - \omega t)]$, with propagation in the x-direction ($k_y = 0$). This implies that $\hat{v}_2 = 0$ and $\hat{\boldsymbol{u}}_2 = \hat{\boldsymbol{u}}_2(z) = [\hat{u}_2(z), 0, \hat{w}_2(z)]$. All other perturbation quantities are represented in a similar manner, with a caret denoting the z-dependent amplitude in each case. From the two components of equation (8) and the definition of ϕ, we obtain the following relation:

$$\hat{w}_2(z) = \frac{g[\gamma_2 - c_2^2 k_x^2/\omega^2]\hat{\phi} - c_2^2 d\hat{\phi}/dz}{\omega^2 - g^2 k_x^2/\omega^2}. \tag{9}$$

The pressure perturbation can also be written in terms of $\hat{\phi}$, using the continuity and energy relations (see Paper I):

$$\hat{p}_2 = -\frac{i\rho_2 c_2^2}{\omega}\left[\frac{(\omega^2 - g^2\gamma_2/c_2^2)\hat{\phi} + g d\hat{\phi}/dz}{\omega^2 - g^2 k_x^2/\omega^2}\right]. \tag{10}$$

Upon substitution of equation (9) into the z-component of equation (8), we obtain the following second-order differential equation for $\hat{\phi}$:

$$\frac{d^2\hat{\phi}}{dz^2} + \left(\frac{1}{c_2^2}\frac{dc_2^2}{dz} - \frac{g\gamma_2}{c_2^2}\right)\frac{d\hat{\phi}}{dz} + \left[\frac{\omega^2}{c_2^2} - k_x^2 + \frac{g^2 k_x^2}{\omega^2 c_2^2}(\gamma_2 - 1) + \frac{g k_x^2}{\omega^2 c_2^2}\frac{dc_2^2}{dz}\right]\hat{\phi} = 0. \tag{11}$$

The nondimensional frequency, horizontal wavenumber, and depth, based on the values of sound speed and density scale height in layer 2 at $z = 0$, are defined by

$$\Omega_2 \equiv H_{20}\omega/c_{20}, \qquad K_2 \equiv H_{20} k_x, \qquad \text{and} \qquad \tilde{z} \equiv z/H_{20}. \tag{12}$$

By transforming the independent and dependent variables according to

$$Y = \frac{2K_2}{\gamma_2 - 1} - 2K_2\tilde{z}, \qquad \psi = e^{Y/2}\hat{\phi}, \tag{13}$$

equation (11) assumes the form

$$Y\frac{d^2\psi}{dY^2} + (b - Y)\frac{d\psi}{dY} - a\psi = 0, \tag{14}$$

where

$$a = \frac{(2\gamma_2 - 1)}{2(\gamma_2 - 1)} - \frac{\Omega_2^2}{2K_2(\gamma_2 - 1)}, \qquad b = \frac{(2\gamma_2 - 1)}{(\gamma_2 - 1)}. \tag{15}$$

Equation (14) is the standard form of Kummer's equation (see Abramowitz and Stegun 1964). The solutions of this equation are given in terms of Kummer's functions,

$$M(a, b; Y) = \frac{\Gamma(b)}{\Gamma(a)}\sum_{n=0}^{\infty}\frac{\Gamma(a + n)}{\Gamma(b + n)}\frac{Y^n}{n!}. \tag{16}$$

The general solution of equation (14) is

$$\psi(Y) = D_3 M(a, b; Y) + D_4 U(a, b; Y), \tag{17}$$

where D_3 and D_4 are arbitrary constants and $U(a, b; Y)$ can be written in terms of Kummer's functions. To insure finite total perturbation energy, we must require that the vertical velocity of the perturbation vanish as $z \to -\infty$ or as $Y \to +\infty$. This in turn requires that $D_3 = 0$. The solution for $\hat{\phi}$ as a function of $\tilde{z}$ in the lower layer is then

$$\hat{\phi}(\tilde{z}) = D_4 \frac{\pi}{\sin \pi b}\exp\left\{-\left[\frac{K_2}{(\gamma_2 - 1)} - K_2\tilde{z}\right]\right\}\left\{\frac{M[a, b; 2K_2/(\gamma_2 - 1) - 2K_2\tilde{z}]}{\Gamma(1 + a - b)\Gamma(b)}\right.$$
$$\left. - \left[\frac{2K_2}{(\gamma_2 - 1)} - 2K_2\tilde{z}\right]^{1-b}\frac{M[1 + a - b, 2 - b; 2K_2/(\gamma_2 - 1) - 2K_2\tilde{z}]}{\Gamma(a)\Gamma(2 - b)}\right\}. \tag{18}$$

The vertical velocity and pressure perturbation are given in terms of $\hat{\phi}$ by equations (9) and (10).

The form of the solution in the upper layer has been given in Paper I, and we shall not repeat the analysis here. The general form for the vertical velocity in the upper layer that gives finite total perturbation energy is given in terms of hypergeometric functions by either

$$\hat{w}_1(z) = D_1 \exp(-zK_1/H_1) F\left[A, B; C; \frac{\Omega_1^2}{\beta^2(K_1^2 - \Omega_1^2)} \exp(-z/H_1)\right] \tag{19}$$

for

$$\left|\frac{\Omega_1^2}{\beta^2(K_1^2 - \Omega_1^2)}\right| < \exp(z/H_1), \tag{20}$$

or else by

$$\begin{aligned}\hat{w}_1(z) = D_1 \exp(-zK_1/H_1)\Bigg\{&\frac{\Gamma(C)\Gamma(B-A)}{[\Gamma(B)]^2}\left[\frac{\beta^2(\Omega_1^2 - K_1^2)}{\Omega_1^2}\right]^A \exp(zA/H_1) \\ &\times F\left[A, 1-B; 1-B+A; \frac{\beta^2(K_1^2 - \Omega_1^2)}{\Omega_1^2}\exp(z/H_1)\right] \\ &+ \frac{\Gamma(C)\Gamma(A-B)}{[\Gamma(A)]^2}\left[\frac{\beta^2(\Omega_1^2 - K_1^2)}{\Omega_1^2}\right]^B \exp(zB/H_1) \\ &\times F\left[B, 1-A; 1-A+B; \frac{\beta^2(K_1^2 - \Omega_1^2)}{\Omega_1^2}\exp(z/H_1)\right]\Bigg\}\end{aligned} \tag{21}$$

for

$$\left|\frac{\Omega_1^2}{\beta^2(K_1^2 - \Omega_1^2)}\right| > \exp(z/H_1). \tag{22}$$

Here

$$A + B = C = 2K_1 + 1, \tag{23}$$

$$AB = \Omega_1^2 + K_1 + \left(\frac{\gamma_1 - 1}{\gamma_1^2}\right)\frac{K_1^2}{\Omega_1^2}, \tag{24}$$

$$\beta^2 = v_0^2/c_1^2, \tag{25}$$

and Ω_1 and K_1 are nondimensional frequency and wavenumber defined as in (12), except sealed with c_1 and H_1.

The pressure perturbation in the upper layer consists of the sum of the gas pressure perturbation and the magnetic pressure perturbation. The gas pressure perturbation can be expressed in terms of the vertical velocity and its derivative as

$$\hat{p}_1 = -i\rho_1 c_1^2 \omega\left(\frac{d\hat{w}_1}{dz} - \frac{g}{c_1^2}\hat{w}_1\right)\Big/(\omega^2 - c_1^2 k_x^2). \tag{26}$$

The magnetic pressure perturbation $\hat{p}_m$ is found from the linearization of

$$p_m + \hat{p}_m = \frac{(\boldsymbol{B}_0 + \hat{\boldsymbol{B}})\cdot(\boldsymbol{B}_0 + \hat{\boldsymbol{B}})}{8\pi},$$

where p_m is the unperturbed magnetic pressure. The components of the perturbed magnetic field are determined by the linearized induction equation (eq. [4] of Paper I). We find

$$\hat{p}_m = -i\frac{v_A^2 \rho_1}{\omega}\frac{d\hat{w}_1}{dz} \tag{27}$$

The total perturbed pressure $\hat{p}_{T_1}$ in layer 1 is expressed in terms of the density and the Alfvén velocity as

$$\hat{p}_{T_1} = -\frac{i\rho_1}{\omega}\left\{[(c_1^2 + v_A^2)\omega^2 - c_1^2 v_A^2 k_x^2]\frac{d\hat{w}_1}{dz} - \omega^2 g\hat{w}_1\right\}\Big/(\omega^2 - c_1^2 k_x^2). \tag{28}$$

IV. EIGENMODES AND RUNNING PENUMBRAL WAVES

We now have expressions for the vertical velocity and the pressure perturbation in each layer of the penumbral model, such that the total perturbation energy is finite. The remaining conditions are the matching of the vertical velocity and the perturbed pressure at the interface $z = 0$.

The scaling of frequency and wavenumber was done separately for each layer in order to simplify the propagation equation as much as possible in each case. In matching across the interface, we need the following relations between parameters in the two layers:

$$H_{20} = \gamma_2(1 + \tfrac{1}{2}\beta^2\gamma_1)H_1 , \tag{29}$$

$$\Omega_2^2 = \gamma_1\gamma_2(1 + \tfrac{1}{2}\beta^2\gamma_1)\Omega_1^2 , \tag{30}$$

$$K_2^2 = \gamma_2^2(1 + \tfrac{1}{2}\beta^2\gamma_1)^2K_1^2 , \tag{31}$$

and equation (7).

Continuity of the vertical velocity across $z = 0$ requires, after normalization, that

$$\hat{w}_1(0) = \hat{w}_2(0) = 1 . \tag{32}$$

This condition fixes the values of the coefficients D_1 in equation (19) or (21) and D_4 in equation (18). The remaining condition, the continuity of the perturbed pressure, requires that we equate (10) and (28). This then leads to the nondimensional condition

$$\left\{\frac{[(1 + \beta^2)\Omega_1^2 - \beta^2K_1^2](d\hat{w}_1/d\tilde{z}_1)|_0 - (\Omega_1^2/\gamma_1)\hat{w}_1(0)}{\Omega_1^2 - K_1^2}\right\} = \frac{1}{\gamma_1}\left[\frac{\Omega_2\gamma_2\tilde{\phi}(0) + (d\tilde{\phi}/dz_2)|_0}{\Omega_2^2 - K_2^2/\Omega_2^2}\right], \tag{33}$$

where $\tilde{\phi} = \hat{\phi}H_{20}$. Equation (33) is only satisfied by particular values of frequency and wavenumber, and gives the dispersion relation for eigenmodes of oscillation in the penumbral model.

In order to evaluate the dispersion relation (33), the free parameters β^2, γ_1 and γ_2 must be specified, which then effectively determines the properties of the model. Although it is possible to evaluate (33) for different values of γ in each layer (for example, a lower value of γ_1 could be taken to represent radiative transfer in the upper layer), we chose the usual value of 5/3 for both layers. The dispersion relation (33) was solved numerically by inserting values of K_1 and then computing and comparing the two sides of (33) for small increments in Ω_1.

Figure 2 shows the first several eigenmodes of the two-layer penumbral model for $\beta^2 = 0.5$ and $\gamma_1 = \gamma_2 = 5/3$. The value of β^2 was chosen to represent a typical penumbra and is slightly less than the value of β^2 at $z = 0$ in our earlier penumbral model (*NT*). Here we have classified the eigenmodes as "plus" or "minus" modes, following the terminology used in the case of an atmosphere with constant spound speed, density scale height, and Alfvén velocity (see McLellan and Winterberg 1968 and NT). The plus modes all lie above the upper dashed line $\Omega = K$ in Figure 2, which corresponds to $\omega = c_1k_x$ (the Lamb mode). The minus mode (there is only one in this case) lies below the lower dashed line $\Omega = \beta K$ which corresponds to $\omega = v_0k_x$. There are no eigenmodes in the region between the dashed lines. This classification of plus or minus modes refers here to the character of the eigenmode

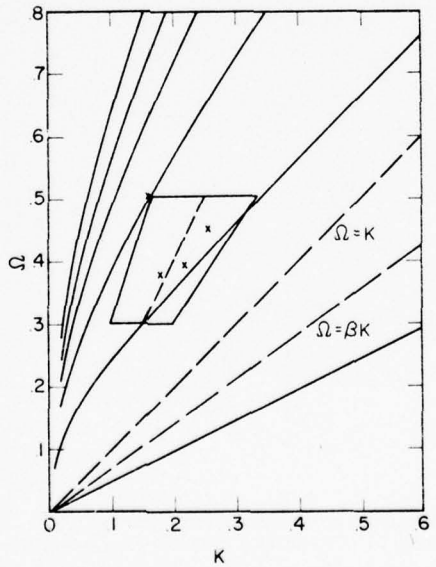

FIG. 2.—The first five plus eigenmodes and the only minus eigenmode of the two-layer penumbral model for $\beta^2 = 0.5$, $\gamma_1 = \gamma_2 = 5/3$. The quadrangle represents the range of observational data (see text). The crosses correspond to particular observations (Giovanelli 1974).

in the upper layer; in the lower layer, all of the modes have the character of acoustic waves (no magnetic field and no buoyancy).

Observational data on penumbral waves are included in Figure 2 for comparison. The most commonly reported observational quantities are the period and the horizontal phase velocity, although they are not always measured simultaneously. Giovanelli (1974) reports a typical phase velocity of running penumbral waves of 15 km s^{-1} and typical periods in the range of 180–240 s. He did report phase velocities of up to 21 km s^{-1}, however, and gave specific periods and wavelengths for four sunspots (denoted by crosses in Fig. 2). The data of Beckers and Schultz (1972) appear to indicate a penumbral oscillation period of 255 s. Moore and Tang (1975) observed penumbral waves with period 270 ± 10 s in a single sunspot. Zirin and Stein (1972) state that the periods of penumbral waves in 20 sunspots were almost all between 240 and 300 s, and the measured horizontal phase velocity of 9.4 km s^{-1} in one spot was more or less the same in other spots even when the period varied.

The quadrangle in Figure 2 represents the range of observations: periods from 180 to 300 s, and phase velocities from 9.4 to 21 km s^{-1}, with a dashed line at 15 km s^{-1} to indicate the value that Giovanelli considers typical. The first plus mode of the penumbral model passes through this quadrangle. Although the particular eigenmode of oscillation of the penumbra is determined by the excitation, the details of which are uncertain, the present results indicate that it is the first plus eigenmode that is being excited. This agrees with our earlier conclusions (NT).

The value $\beta^2 = 0.5$ used in Figure 2 was chosen to represent a typical penumbra. In Figure 3 the effect of changes in β^2 on the first plus mode is shown for a range of β^2 of two orders of magnitude (0.05, 0.5, 5.0). This constitutes a reasonable set of limits on β^2 for penumbral conditions, and is obtained by looking at the normal variation of B (factor of 4), ρ (factor of 4), and c^2 (factor of 1.5) expected in different penumbrae. We see that for any reasonable value of β^2, the penumbral model has a first plus mode within the range of observations.

The vertical distributions of velocity and kinetic energy of the first plus mode (for $\beta^2 = 0.5$) are shown in Figure 4 for $K_1 = 0.1995$ and $\Omega_1 = 0.3628$, corresponding to a horizontal wavelength $\lambda = 3{,}000$ km and period $\tau = 250$ s for $c_1^2 = 43.5$ km^2 s^{-2}. Here the nondimensional height is scaled everywhere by the density scale height in the upper layer, H_1. The velocity distribution is fairly symmetric, with the maximum amplitude occurring slightly above $z = 0$ in the penumbral photosphere. The kinetic energy, on the other hand, is almost entirely trapped in the lower layer (convection zone)with maximum energy just below the interface. The velocity amplitude decays slowly with height with a value of more than 25 percent of the maximum amplitude at a distance of 8 scale heights above the level of that maximum.

There is a discrepancy between the height of maximum velocity predicted here ($z \approx 100$ km) and that predicted in our earlier paper (NT, $z \approx 1000$ km). Here the Alfvén velocity increases exponentially with height above the photosphere, whereas in NT it increased linearly. Thus, the downward refraction of waves is much stronger in the

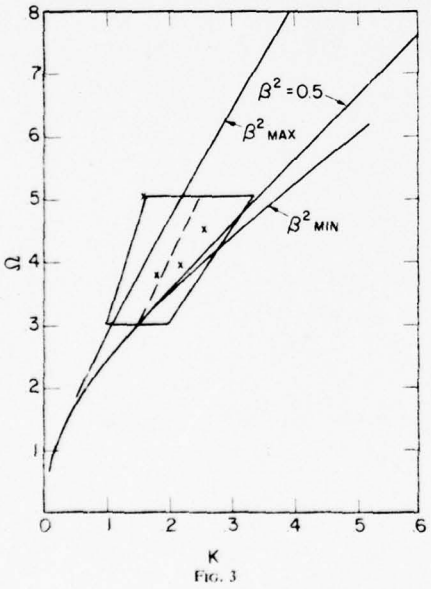

FIG. 3

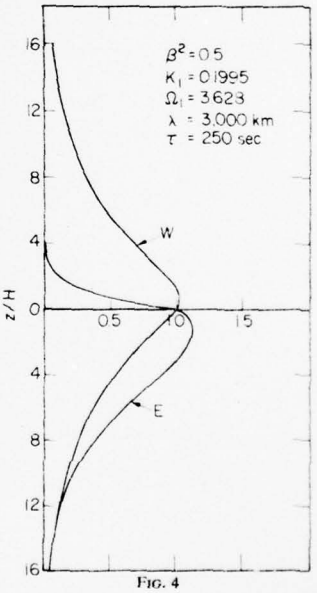

FIG. 4

FIG. 3.—The first plus eigenmode evaluated for extreme values of β^2 for sunspot penumbrae (see text): $\beta_{max}^2 = 5.0$, $\beta_{min}^2 = 0.05$. The quadrangle represents the range of observational data. The crosses correspond to particular observations (Giovanelli 1974).

FIG. 4.—The distribution of vertical velocity and kinetic energy of the first plus eigenmode with nondimensional height z/H_1. The velocity and energy are each normalized to value unity at the interface $z/H_1 = 0$.

present model. The actual situation is probably somewhere between these two cases. In either case, the wave energy lies mostly below the height of maximum vertical velocity, in the convection zone and low photosphere.

V. CONCLUSIONS

The present results, taken together with our earlier work (NT), indicate that running penumbral waves should be identified with the lowest plus mode of trapped magneto-atmospheric waves in the penumbra. The vertical trapping is primarily due to the increasing Alfvén velocity up into the chromosphere and the increasing sound speed down into the convection zone. Most of the energy of the penumbral waves lies in the convection zone and low photosphere, at the same level as the expected source of excitation (umbral oscillatory convection). The maximum wave amplitude occurs somewhat higher.

The results also indicate that penumbral waves should be observable in a photospheric spectral line (see Fig. 4) as well as in Hα. There is some indication of this in the observation of Beckers and Schultz (1972). Their data show a 255 s period oscillation in the penumbra of one sunspot observed in a photospheric line. They present contours of vertical velocity as a function of horizontal position and time (their Fig. 1) in which one may note horizontal propagation outward across the penumbra at about the right phase speed. We plan further observations in a search for penumbral waves in the photosphere.

Much of this work was done while we were guests of the Max-Planck-Institut für Physik und Astrophysik in München, Germany. We are grateful to Professor Biermann for the hospitality of the Institut, and to Drs. H. U. Schmidt, Friedrich Meyer, John Stewart, and Tadashi Hirayama for helpful discussions. We also thank Professor Alfred Clark, Jr., at Rochester for helpful comments. One of us (A. H. N.) was supported by a National Science Foundation Predoctoral Traineeship. This work was supported by Air Force contract F 19628-75-C-0011 through Sacramento Peak Observatory, and by the Office of Naval Research.

REFERENCES

Abramowitz, M., and Stegun, I. A. 1964, ed., *Handbook of Mathematical Functions* (Washington: National Bureau of Standards), p. 503.
Beckers, J. M., and Schultz, R. B. 1972, *Solar Phys.*, **27**, 61.
Bray, R. J., and Loughhead, R. E. 1964, *Sunspots* (London: Chapman & Hall), p. 212.
Giovanelli, R. G. 1972, *Solar Phys.*, **27**, 71.
———. 1974, in *IAU Symposium 56, Chromospheric Fine Structure*, ed. R. Grant Athay (Dordrecht: Reidel), p. 137.
Leibacher, J. W. 1971, Ph.D. thesis, Harvard University.
McLellan, A., and Winterberg, F. 1968, *Solar Phys.*, **4**, 401.
Moore, R. L. 1973, *Solar Phys.*, **30**, 403.
Moore, R. L., and Tang, F. 1975, *Solar Phys.*, **41**, 81.
Nishi, K., and Makita, M. 1973, *Pub. Astr. Soc. Japan*, **25**, 51.
Nye, A. H., and Thomas, J. H. 1974, *Solar Phys.*, **38**, 399 (NT).
———. 1976, *Ap. J.*, **204**, 573 (Paper I).
Zirin, H., and Stein, A. 1972, *Ap. J. (Letters)*, **173**, L85.

ALAN H. NYE: Sacramento Peak Observatory, Sunspot, NM 88349

JOHN H. THOMAS: Department of Mechanical and Aerospace Sciences, University of Rochester, Rochester, NY 14627

THE ASTROPHYSICAL JOURNAL, 206:L175–L178, 1976 June 15

OBSERVATIONS OF PENUMBRAL WAVES IN THE PHOTOSPHERE

STEVEN MUSMAN AND ALAN H. NYE*
Sacramento Peak Observatory, Air Force Geophysics Laboratory
AND
JOHN H. THOMAS†
Department of Mechanical and Aerospace Sciences, University of Rochester
Received 1976 February 10; revised 1976 March 23

ABSTRACT

Simultaneous observations have been made of velocities in the chromosphere (in Hα) and in the photosphere (in the nonmagnetic Fe I line λ5576) of three sunspots. The results reveal waves propagating horizontally outward across the penumbra in the photosphere with about the same period as the running penumbral waves in Hα (250–290 s). The photospheric waves are more intermittent and have higher horizontal phase velocity (by a factor of 2 or more) than the chromospheric penumbral waves.

Subject headings: hydromagnetics — Sun: atmospheric motions — Sun: sunspots

I. INTRODUCTION

One of the most interesting recent discoveries concerning the dynamics of the solar atmosphere is that of waves observed in Hα that propagate outward across sunspot penumbrae. These "running penumbral waves" (or simply "penumbral waves") were discovered independently by Zirin and Stein (1972) and by Giovanelli (1972, 1974). They are often seen in large sunspots with a stable, regular penumbra, and their observed horizontal phase velocities are in the range 8–25 km s^{-1}, periods in the range 150–270 s, and horizontal wavelengths in the range 2300–3800 km. The associated motions are largely vertical (i.e., normal to the solar surface).

The nature of the wave motion indicates that compressibility, buoyancy, and magnetic field all play a role in penumbral waves. The observed phase velocities are indicative of conditions in the penumbral photosphere rather than the chromosphere. (For example, the Alfvén speed at height of formation of Hα is much larger than 25 km s^{-1}). This suggests that penumbral waves are a photospheric phenomenon. We have given a theoretical description (Nye and Thomas 1974, 1976) of penumbral waves as magnetoatmospheric waves that are vertically trapped at photospheric levels, the trapping being due to refraction by the increasing Alfvén speed up into the chromosphere and the increasing sound speed down into the convection zone. The waves are evanescent at heights of formation of Hα, but have their largest amplitude there due to the rapid decrease in density with height. The wave energy is mostly in the photosphere and subphotosphere, which is also the location of the probable source of excitation of the waves, namely, overstable convection in the umbra (Musman 1967; Savage 1969; Moore 1973).

For a maximum vertical velocity of order 1 km s^{-1} in Hα (Giovanelli 1974), the theory (Nye and Thomas 1974, 1976) predicts vertical velocities of order 100 m s^{-1} or greater in the photosphere; thus, penumbral waves should also be observable in a photospheric spectral line. This prediction prompted the simultaneous photospheric and chromospheric observations reported here.

II. OBSERVATIONS

We used the Sacramento Peak vacuum tower telescope (Dunn 1969), echelle spectrograph (Dunn 1971) and the diode array (Dunn and Spence 1973) to obtain spectral scans in a manner similar to that of Musman (1974). At each position of a two-dimensional raster we recorded on magnetic tape the intensity measured at 40 equally spaced wavelengths in a spectral interval of 1 Å centered about the nonmagnetic line of Fe I at λ5576.099. This line is formed in the upper penumbral photosphere. Altrock *et al.* (1975) state that in the quiet photosphere 90 percent of the line center contribution function is formed between 250 and 530 km above optical depth unity at 5000 Å. We assume a similar behavior for the penumbra. Each measurement is limited by a 1″ (700 km) aperture and is performed in 2/15 of a second. Each scan line contains 40 positions with 1″ spacing. Each raster contains three adjacent lines with 1″ spacing and takes 25.4 s to complete. The raster was positioned visually such that the center scan line passed through the center of the sunspot umbra in each observation; in this way, propagation along the scan lines corresponds to radial propagation across the sunspot. A typical run consisted of 64 scans covering a time period of 27 minutes. After each scan the image is returned to the center of the raster and an Hα photograph of the slit jaws is taken. This process occupies about 5 s of the total scan time. These Hα photographs were later combined to form a movie.

Velocities are obtained by locating the center of the

* National Research Council Resident Research Associate.
† Also with C. E. Kenneth Mees Observatory.

line profile by interpolation on a smoothed line profile as described by Musman (1974). All velocities are referred to the mean velocity of each raster. We averaged the velocities of the three adjacent lines in order to suppress the noise in a single measurement and obtained the equivalent of one 40-point scan line. Since the velocity is measured at a slightly different time and we scan an odd number of lines in alternate directions, a perfectly uniform oscillatory pattern on the Sun could give rise to an apparent phase velocity in the direction of scanning of the odd-numbered lines. However this apparent phase velocity is greater than 3000 km s^{-1} and introduces a negligible error in measuring phase velocities two orders of magnitude smaller.

We observed two sunspots in McMath regions 13875 and 13890 on 1975 October 5–9 and October 16–19. Preliminary observations were also obtained for a sunspot in McMath region 13738 on 1975 June 28–July 1, but detailed results will be given here only for the later two spots.

III. RESULTS

a) Chromosphere

When the Hα slit-jaw pictures are projected as a movie, the running penumbral waves are most conspicuous for McMath region 13875. The waves appear continuously for all observations of this sunspot over a period of 5 days. They have an average period of 240 ± 10 s and propagation velocities in the range from 10–18 km s^{-1}. These waves then appear to be typical, consistent with the observations of Zirin and Stein (1972) and Giovanelli (1972, 1974).

On viewing the Hα movie of McMath region 13890, one has the impression of waves propagating outward across the penumbra, but the pattern is not distinct enough to make measurements of periods or velocities. There is no indication of running penumbral waves in McMath region 13738, but the time interval between pictures is longer in that observation, making the waves more difficult to detect.

b) Photosphere

To determine the reliability of the λ5576 velocity data, it was first necessary to determine the noise in the signal. To do this, a series of scans was made out of focus, giving a uniform solar signal. From this the noise was found to have nearly equal power at all frequencies with rms velocity on the order of 26 m s^{-1}. We also measured a nearly uniform spectrograph drift of 21 mÅ hr^{-1}. The average value of each scan was subtracted to remove the effect of the spectrograph drift. Next, the time series for each of the 40 points in the scan was analyzed. The mean for each time series was removed. This eliminated the conspicuous effect of Evershed flow. The best estimate of the true signal was obtained by using a bandpass filter in the manner described by Brault and White (1971). The filter removed high-frequency (period < 70 s) noise plus a very low-frequency (period > 800 s) drift due to an instrumental problem in the diode array. The power spectra for the unfiltered data are essentially flat for high frequencies, which is indicative of white noise and consistent with the out-of-focus data.

The filtered data clearly show 5-minute oscillations in the portion of the scan outside of the spot. The data also show 5-minute oscillations in the umbra, with typical amplitudes of 50 m s^{-1}; but since these are usually 180° out of phase with the oscillations outside the spot, we suspect that this is a systematic error due to referring all velocities to the average of each scan. Repeating one of the scans with a velocity referenced to the average umbral velocity in an attempt to remove this effect does not significantly change the results reported below. The error in velocity reference is opposite to the effect of scattered light, which would give oscillations in phase. We looked primarily for horizontally propagating waves in the penumbra resembling those observed in Hα. Neither scattered light nor an inaccurate velocity reference could introduce such a systematic propagation.

The filtered data show oscillations in the penumbral photosphere, but not in the form of a continuous outward-propagating wave train sometimes seen in Hα. There do appear, on four occasions, what we term penumbral photospheric events. These are isolated wave packets that propagate outward across the penumbra. The packets consist of one or two complete oscillations whose period (250–290 s) is comparable to that of the chromospheric penumbral waves. Figure 1 shows an example of one such event, as illustrated by the time history of the line-of-sight velocity at each scan point across the penumbra. The heliocentric angle of the sun-

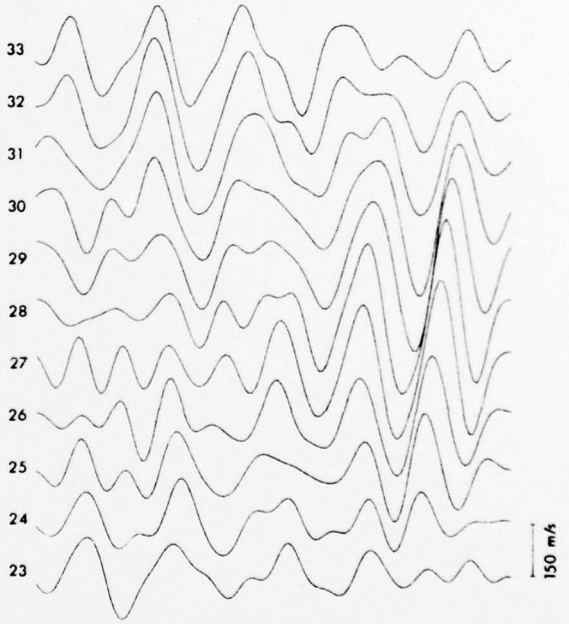

FIG. 1.—An example of a penumbral photospheric event (event 3 in Table 1). The time records of the filtered velocity signal at points across the penumbra are shown. The numbered scan positions (with 1″ spacing) correspond to those shown in Fig. 2.

spot during each of the four events was roughly 30°, so that line-of-sight velocities were predominantly vertical. The amplitude of each of the four events is nearly an order of magnitude larger than the rms noise. There may have been a fifth event in McMath region 13738, but it occurred too near the beginning of the record to be identified unambiguously.

The horizontal phase velocities of the four events are in the range 37–90 km s^{-1}. Individual phase velocities, amplitudes, periods, locations, dates, and times of the four events are listed in Table 1. The locations given in Table 1 refer to the numbered positions across the sunspot shown in Figure 2, which also shows plots of the continuum intensity across the scan. The times given in Table 1 refer to the central time of each event. This is the time when the maximum amplitude of each wave packet passed the central location in its range of propagation. The periods listed in Table 1 are consistent with the data of Beckers and Schultz (1972), who found power at 255 s in the penumbral photosphere of the sunspot they studied.

To determine whether these penumbral photospheric events could have been due to chance, we calculated the probability that the phase of a sequence of independent oscillators with the same frequency but random phase could combine to form an apparently propagating wave. This type of problem has been treated by Roach (1968). The probability of having the phase differences of five random oscillators out of 40 within 20° is 5×10^{-4}. We analyzed in detail six independent sets of data from six different days and two sunspots, for a total time of 2.7 hours. All four events extended over five to seven positions and are statistically significant.

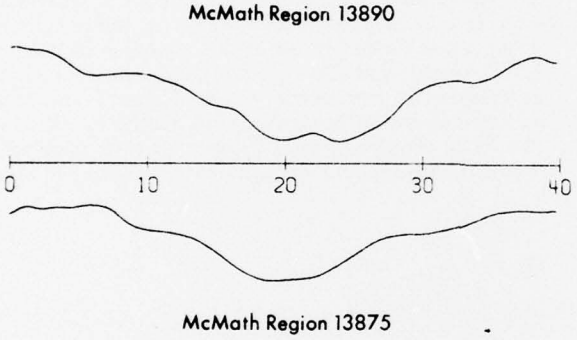

FIG. 2.—Continuum intensity versus position across the scan for the two sunspots in Table 1. The numbered scan positions (0–40) have 1″ spacing.

IV. CONCLUSIONS

Our observations at chromospheric and photospheric levels in three sunspots lead us to the following conclusions:

1. Typical running penumbral waves were observed at chromospheric levels.

2. At photospheric levels we observed statistically significant events consisting of isolated wave packets (one or two complete oscillations) propagating outward across the penumbra. Four events were seen during 2.7 hours of observation. The period of these oscillations is comparable to that of the penumbral waves in Hα. The existence of these events is a partial confirmation of the prediction of Nye and Thomas (1974, 1976).

3. The waves observed in the penumbral photosphere are more intermittent and have higher horizontal phase velocity (by a factor of 2 or 3 or more) than the penumbral waves in Hα. Thus, the connection (if any) between the penumbral photospheric events and the chromospheric penumbral waves is unclear at present, and in any event is more complicated than the resonant mode model of Nye and Thomas (1976).

We thank G. Richard Mann, Horst Mauter, and Howard DeMastus for help with the observations. Jacques M. Beckers provided valuable criticism of the manuscript. J. H. Thomas was supported by Air Force contract F 19628-75-C-0011 through Sacramento Peak Observatory.

TABLE 1

PARAMETERS FOR THE PHOTOSPHERIC PENUMBRAL EVENTS

Event	Sunspot	Location*	Horizontal Phase Velocity (km s^{-1})	Amplitude (m s^{-1})	Period (s)	Date and Time (UT)†
1.....	13875	21–27	90	220	264	10/6/75, 14:27:52
2.....	13875	11–7	64	255	258	10/6/75, 14:22:08
3.....	13890	25–31	37.5	265	252	10/16/75, 14:42:54
4.....	13890	18–13	47	170	290	10/16/75, 14:26:53

* Location refers to the numbered scan positions in Fig. 2.

† Time refers to the central time of the event.

REFERENCES

Altrock, R. C., November, L. J., Simon, G. W., Milkey, R. W., and Worden, S. P. 1975, *Solar Phys.*, **43**, 33.
Beckers, J. M., and Schultz, R. B. 1972, *Solar Phys.*, **27**, 61.
Brault, J. W., and White, O. R. 1971, *Astr. and Ap.*, **13**, 169.
Dunn, R. B. 1969, *Sky and Tel.*, **38**, 368.
———. 1971, in *The Menzel Symposium on Solar Physics, Atomic Spectra, and Gaseous Nebulae*, ed. K. B. Gebbie (NBS Spec. Pub. No. 353), p. 71.
Dunn, R. B., and Spence, G. E. 1973, *Bull. AAS*, **5**, 271.
Giovanelli, R. G. 1972, *Solar Phys.*, **27**, 71.
———. 1974, in *IAU Symposium No. 56, Chromospheric Fine Structure*, ed. R. G. Athay (Dordrecht: Reidel), p. 137.
Moore, R. L. 1973, *Solar Phys.*, **30**, 403.
Musman, S. 1967, *Ap. J.*, **149**, 201.
———. 1974, *Solar Phys.*, **36**, 313.
Nye, A. H., and Thomas, J. H. 1974, *Solar Phys.*, **38**, 399.
———. 1976, *Ap. J.*, **204**, 582.
Roach, S. A. 1968, *The Theory of Random Clumping* (London: Methuen), p. 6.
Savage, B. D. 1969, *Ap. J.*, **156**, 707.
Zirin, H., and Stein, A. 1972, *Ap. J.* (*Letters*), **178**, L85.

STEVEN MUSMAN and ALAN H. NYE: Sacramento Peak Observatory, Sunspot, NM 88349

JOHN N. THOMAS: Department of Mechanical and Aerospace Sciences, University of Rochester, Rochester, NY 14627

SOLAR MAGNETO-ATMOSPHERIC WAVES

John H. Thomas

Department of Mechanical and Aerospace Sciences

and

C.E. Kenneth Mees Observatory

University of Rochester

Rochester, New York 14627, U.S.A.

(Paper to be presented at IAU Colloquium 36, "Energy Balance and Hydrodynamics of the Chromosphere and Corona," Nice, France, September 6-10, 1976)

* * * * *

I would like to say a few words about the theory of what I call magneto-atmospheric waves, which also go under the name of magneto-acoustic-gravity waves. These are waves that involve the combined restoring forces due to compressibility, gravity, and the magnetic field. For many waves observed in the solar atmosphere, all three of these effects are important.

Nearly all work on magneto-atmospheric waves has been based on linearized theory for a plane-stratified, nondissipative atmosphere. (See Chiu 1971 for a discussion of the nonlinear case.) Wave propagation is then determined by the vertical distribution of three parameters: the sound speed c, the Alfvén speed v_A, and the local density scale height H. The theory is complicated by the fact that the medium is both

anisotropic and inhomogeneous. Gravity and the magnetic field each introduce a preferred direction. The inhomogeneity influences wave propagation most strongly through the rapid increase of the Alfvén speed with height.

The simplest approach to atmospheric wave problems is to find a dispersion relation for plane waves. However, this approach has not been very fruitful for solar magneto-atmospheric waves. Unless all three wave parameters c, v_A, and H are constant with height, we can find only a "local" dispersion relation (MacDonald 1961; McLellan and Winterberg 1968; see also Bel and Mein 1971; Michalitsanos 1973; Nakagawa et al. 1973; Yeh 1974) that holds only for waves whose vertical wavelength is much smaller than the smallest scale height of the undisturbed atmosphere. We can see how restrictive this approach is by recalling that in the photosphere and much of the chromosphere the density scale height is smaller than our limit of observational resolution.

There is one special case, first studied by C.P. Yu (1965; see also Chen and Lykoudis 1972; Nye and Thomas 1974), in which c, v_A, and H are all constant. This is the case of an isothermal atmosphere with a horizontal magnetic field that decreases exponentially with height as $\exp(-z/2H)$. This leads to a global dispersion relation. However, magnetic fields on the sun usually vary more slowly than the density, so this case has limited applicability.

Perhaps the simplest model atmosphere for solar magneto-atmospheric waves is an isothermal atmosphere with a uniform magnetic field. In this case the sound speed c and the density scale height H are constant,

but the Alfvén speed increases exponentially with height as $e^{z/2H}$. This rapid increase of Alfvén speed with height causes strong refraction and downward reflection of waves, which can not be adequately discussed with the local dispersion relation. We must go back to the basic wave equations with variable coefficients, for which solutions have been found in certain cases.

Approximate solutions for the case of a uniform vertical magnetic field were first given by Ferraro and Plumpton (1958; see also Weymann and Howard 1958; Stepien 1967). There are three types of wave modes in this case. One is an Alfvén wave having only nondivergent horizontal motions. The other two modes have both vertical and horizontal motions, and may be described as gravity-modified magneto-acoustic waves, or as magnetically-modified acoustic-gravity waves, depending on the relative valves of the sound speed and Alfvén speed at some reference level. Meyer (1968) used an approximate solution similar to Ferraro and Plumpton's in a model for flare-induced coronal waves, or Moreton waves. In his model the chromosphere-corona transition region provides a lower reflective boundary, and the resulting trapped modes of gravity-modified fast waves are identified with the coronal waves.

For the case of an isothermal atmosphere with a uniform horizontal magnetic field, Alan Nye and I (Nye and Thomas 1976a) have recently given an exact solution for the wave modes. The wave equation in this case transforms to the hypergeometric equation, and solutions can be expressed in terms of hypergeometric functions. We applied this solution to a model of flare-induced coronal waves similar to Meyer's,

but with the magnetic field horizontal instead of vertical. The resulting trapped modes propagate horizontally, with very little dispersion for all horizontal wavelengths less than about 100,000 km (see Fig. 1). Thus a flare-induced pulse will propagate horizontally over large distances with little distortion, as is indeed observed.

We have also used our exact solution in a model for running penumbral waves (Nye and Thomas 1976b). The model consists of an upper isothermal layer with a uniform horizontal magnetic field, representing the penumbral photosphere and low chromosphere, and a lower adiabatic layer with no magnetic field, representing the underlying convection zone. The penumbral waves are identified with fast modes that are trapped by the increasing Alfvén speed above and the increasing sound speed in the convection zone below. Figure 2 is a diagnostic diagram showing computed eigenmodes for a typical penumbra, along with the range of observed frequency and wavelength of penumbral waves. There is good agreement between observations and the lowest eigenmode. Based on the form of the eigenmode, the theory predicts that penumbral waves, which were discovered in $H\alpha$, should also be observable in the photosphere. This prediction was recently confirmed by Steve Musman, Alan Nye, and myself (Musman, Nye, and Thomas 1976) in observations with the tower telescope and diode array at Sacramento Peak Observatory.

I want to mention briefly one other aspect of magneto-atmospheric waves which I have been working on recently. In the case of a horizontal magnetic field there is a singularity in the basic wave equation at a

height at which

$$\frac{\omega}{k_x} = \left[\frac{c^2 v_A^2}{c^2 + v_A^2}\right]^{1/2} .$$

When c or v_A, or both, vary with height, then for slow waves of a certain frequency ω and horizontal wavenumber k_x there exists a critical height z_c at which this relation is satisfied. In the local, or WKB approximation, the vertical wavenumber becomes infinite at the critical level, and waves take an infinite time to reach this level; thus, the critical level acts as an absorbing barrier for waves. But in fact the WKB approximation breaks down at the critical level, so this is not an adequate discussion.

This phenomenon is similar to the critical levels that occur in the stability of inviscid shear flow (Lin 1966) and in the propagation of internal gravity waves in a shear flow (Booker and Bretherton 1967). In the present case the singularity is logarithmic and the singular point is thus a branch point. We can use the technique of Booker and Bretherton to decide on the proper branch of the solutions and to connect solutions above and below the critical level. The conclusion is that waves are not completely absorbed, but are attenuated as they pass through the critical level. The attenuation is algebraic, rather than exponential as in the case of internal gravity waves in a shear flow. Energy is absorbed by the mean magnetic field. If the undisturbed magnetic field is slightly inclined to the horizontal, the attenuation is reduced. The critical level phenomenon may be of importance in the energy balance of the chromosphere and corona.

My own research on magneto-atmospheric waves has been supported by Air Force Contract F 19628-75-C-0011 through Sacramento Peak Observatory.

References

Bel, N., and Mein, P. 1971, Astron. Astrophys. 11, 234-240.

Booker, J.R., and Bretherton, F.P. 1967, J. Fluid Mech. 27, 513-539.

Chen, C.-J., and Lykoudis, P.S. 1972, Solar Phys. 25, 380-401.

Chiu, Y.T. 1971, Phys. Fluids 14, 1717-1724.

Ferraro, V.C.A., and Plumpton, C. 1958, Astrophys. J. 127, 459-476.

Lin, C.C. 1966, The Theory of Hydrodynamic Stability, Cambridge University Press.

MacDonald, G.J.F. 1961, J. Geophys. Res. 66, 3639-3670.

McLellan, A., and Winterberg, F. 1968, Solar Phys. 4, 401-408.

Meyer, F. 1968, in IAU Symposium 35, Structure and Development of Solar Active Regions, ed. K. Kiepenheuer (Dordrecht: Reidel), pp 485-489.

Michalitsanos, A.G. 1973, Solar Phys. 30, 47-61.

Musman, S., Nye, A.H., and Thomas, J.H. 1976, Astrophys. J. (Letters) 206, L175-L178.

Nakagawa, Y. Priest, E.R., and Wellck, R.E. 1973, Astrophys, J. 184, 931-953.

Nye, A.H., and Thomas, J.H. 1974, Solar Phys. 38, 399-413.

Nye, A.H., and Thomas, J.H. 1976a, Astrophys. J. 204, 573-581.

Nye, A.H., and Thomas, J.H. 1976b, Astrophys. J. 204, 582-588.

Stepien, K. 1967, Acta Astron. 17, 31-54.

Weymann, R., and Howard, R. 1958, Astrophys. J. 128, 142-145.

Yeh, T. 1974, Phys. Fluids 17, 2282-2289.

Yu, C.P. 1965, Phys. Fluids 8, 650-656.

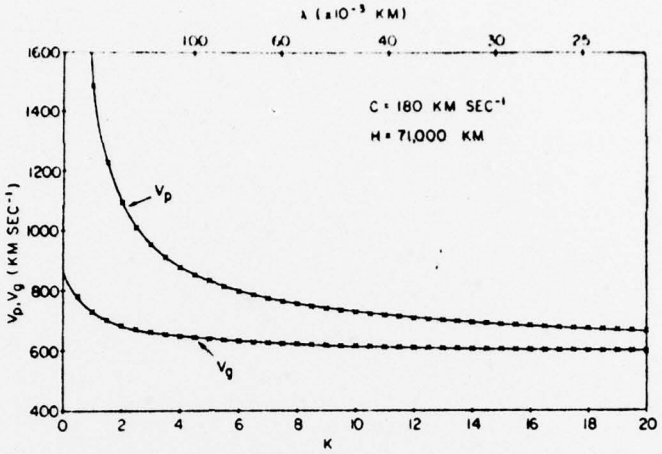

FIG. 1—Phase velocity v_p and group velocity v_g of the first mode of coronal oscillation plotted as a function of horizontal wavenumber.

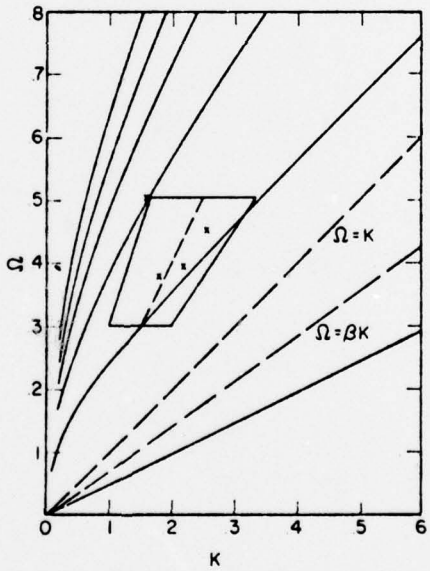

FIG. 2.—The first five plus eigenmodes and the only minus eigenmode of the two-layer penumbral model for $\beta^2 = 0.5$, $\gamma_1 = \gamma_2 = 5/3$. The quadrangle represents the range of observational data (see text). The crosses correspond to particular observations (Giovanelli 1974).

Printed by
United States Air Force
Hanscom AFB, Mass. 01731